Design of Singlet Fission Chromophores through the Introduction of N-Oxyl Fragments

Dylan James

A Thesis submitted to the Faculty of Graduate Studies in Partial Fulfillment of the Requirements for the Degree of Master of Science

Graduate Program in Chemistry
York University,
Toronto, Ontario

September, 2022

Abstract

Singlet fission is a highly desired phenomenon in photovoltaics. In the fission process, one short-lived singlet exciton splits to two long-lived triplet excitons. Generating a larger number of longer-lived excitons, singlet fission has the potential to enhance the photoelectric conversion efficiency. The exploitation of this phenomenon in the photovoltaic industry is however impacted by the small pool of existing singlet fission chromophores. Here, we report on the design of novel singlet fission chromophores through the substitution of N-oxyl fragments within the anthracene framework. The substantial diradical character brought on by the N-oxyl fragments located at specific positions on the anthracene pristine structure together with structural reorganization induced by excitation allows for a handful of chromophores to satisfy the thermodynamic requirements of singlet fission.

Acknowledgements

The completion of this thesis and the corresponding research would not have been possible without the guidance and knowledge of Dr. Tao Zeng. I would also like to thank Dr. René Fournier and Dr. Christopher Caputo for their support throughout this thesis.

A debt of gratitude is also owed to Dr. Ekadashi Pradhan for his help with navigating through the GAMESS-US and ORCA software packages.

Table of Contents

List of Tables

List of Figures

Chapter 1: Introduction

1.1: Singlet Fission

The incidence of a solar photon onto the chromophore layer of an organic photovoltaic (OPV) device creates a singlet exciton. This exciton migrates to the chromophore-acceptor interface, where the exciton undergoes charge separation to form an electron and a hole. The hole and electron are collected at electrodes as free charge carriers. Such a desired evolution of excitons is impeded by competing channels, e.g., the singlet excitons decaying to the ground state via radiative or radiationless channels, emitting heat and light respectively. These detrimental channels impose the Schockley-Queisser limit of 33% onto the photoelectric conversion efficiency (PCE) for single p-n-junction solar cells[1]. In 2005, Hanna and Nozik introduced carrier multiplication as a mechanism to increase the PCE of organic photovoltaics to roughly 45%[2]. Singlet fission (SF), first discovered by the delayed fluorescence of anthracene, is an archetype of carrier multiplication[3]. An organic chromophore in the singlet excited state can share its energy with a neighboring chromophore in the ground state, resulting in two triplet excitons on both chromophores[4-6]. In addition to such a number doubling of excitons, the triplet excitons usually have longer lifetimes than the singlet counterparts, because the aforementioned radiationless and radiative decay channels for singlet excitons are not applicable to triplet excitons, due to their spin-conserved selection rules. The triplet excitons are therefore more likely to reach the chromophore/acceptor interface and undergo charge separation to provide free charge carriers. Therefore, singlet fission has the potential to enhance the PCE in OPV devices[7]. The mechanisms of OPV devices with and without singlet fission are compared in **Figure 1**.

The two triplet excitons on neighboring chromophores are coupled to form an overall singlet[8-10]. Therefore, SF is intrinsically an internal conversion process within the singlet manifold of excited states. The generation of the triplet excitons does not go through intersystem crossing, which usually involves environment-unfriendly heavy element compounds. This is another merit of SF.

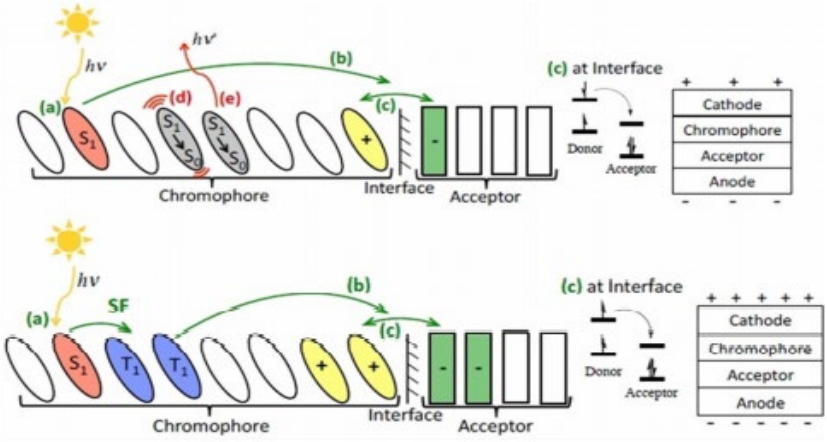

Figure 1: Schematics of photoelectric conversions with (lower panel) and without (upper panel) singlet fission. Adapted from Ref. 11, copyright 2018 John Wiley and Sons.

The exploitation of SF in the OPV industry is however hindered by the lack of chromophores that can undergo this process[11-13]. There are three fundamental thermodynamic requirements for SF chromophores to satisfy[4,5,14]. These requirements manifest in the three inequalities shown below:

$$E(S1) > 2E(T1) \quad Eq.(1)$$

$$E(T2) > 2E(T1) \quad Eq.(2)$$

$$E(Q1) > 2E(T1) \quad Eq.(3)$$

The subscripted numbers index the energy order within each spin manifold: S_1 for the first singlet excited state, T_2 for the second triplet excited state, etc. Throughout this thesis, "S_0" is used to

indicate the singlet ground state. Eq. (1) is arguably the most important, as it determines the thermodynamic driving force for the fission of one S_1 state to two T_1 states, in the generation of the coupled triplet pair, ^{1}TT. Eqs. (2) and (3) provide endoergic hindrances to prevent triplet fusion, forming a triplet exciton (T_2) or quintet exciton (Q_1) in one chromophore. The Q_1 state is usually higher in energy than the T_2 or S_1 states. This is because Q_1 usually involves a two-electron excitation, from HOMO and HOMO-1 to LUMO and LUMO+1, while T_2 and S_1 usually involve one-electron excitations only. HOMO and LUMO stand for highest occupied and lowest unoccupied molecular orbitals, respectively. As such, Eq. (3) is automatically satisfied if the conditions for Eqs. (1) and (2) are met. Eq. (3) can thus be ignored when discussing the thermodynamic requirements for SF chromophores.

Looking at the frontier orbitals, a T_2 excitation usually involves one-electron excitation from the HOMO-1/HOMO to LUMO/LUMO+1 respectively, while a S_1 excitation, at least for the chromophores we are considering, involves a HOMO-LUMO excitation. Given the orbital energy differences, the T_2 state is usually higher in energy than the S_1 state. However, this is not always the case. While Eq. (2) does play a role, it comes secondary to Eq. (1). Overall, Eq. (1) is the primary thermodynamic criterion for SF chromophores. Unfortunately, there are only a handful of known molecules that satisfy Eq. (1), and even fewer that satisfy both Eqs. (1) and (2). The desire for exploiting SF in the OPV industry and the fact of lacking chromophores together motivate a research front in materials science in designing SF chromophores. This is the main theme of the present thesis.

1.2: Early Search for Singlet Fission Chromophores

The search for SF chromophores using computational chemistry was inspired by Paci et al. in 2006[15]. They concluded that SF chromophores can be derived from two types of molecules, polycyclic alternant hydrocarbons (PACs) and diradicals. In 2011, Minami and Nakano unified the two routes of designing SF chromophores starting from the two types of parent structures and pointed out that diradical character is the only factor that matters[16-19].

1.3: Diradical Character

Minami and Nakano chose the linear H_4 system to demonstrate the relationship between singlet fission excitation energies and diradical and tetraradical characters (symbolized as y_0 for diradical character and y_1 for tetraradical character)[16]. Through adjusting the internuclear distances of the linear H_4 system, Minami and Nakano tuned the diradical and tetraradical characters at the ground state. The simplicity of this system allows for $E(S_0)$, $E(S_1)$, $E(T_1)$ and $E(T_2)$ to be evaluated to a high accuracy. The thermodynamics criteria for SF chromophores, namely $E(S_1) > 2E(T_1)$ and $E(T_2) > 2E(T_1)$, were assessed for the H_4 model and associated to the diradical and tetraradical characters of the molecule. Here, the diradical character index y_0 is directly taken as the occupancy of the lowest unoccupied natural orbital (LUNO), and the tetraradical character index y_1 is taken as the occupancy of the second-lowest unoccupied natural orbital (LUNO+1). Through direct comparison of the natural occupancies and excited state energies, Minami and Nakano were able to reveal the link between diradical character and singlet fission. They determined that a large diradical character is the key to satisfy Eq. (1), yet too large diradical character implies instability. Therefore, sufficient, not a lot nor a little, diradical character in the ground state is desired for SF

chromophores. On the other hand, a high tetraradical character implies a low E(T_2), and thus the risk of dissatisfying Eq. (2). Therefore, a low tetraradical character is desirable for SF chromophores.

A more quantitative relation between diradical character and the satisfaction of Eq. (1) was proposed by Minami et al. in 2013[21]. They employed a two-site model, which is shown in **Figure 2**. The two localized orbitals *a* and *b* overlap and interact to form the bonding and antibonding molecular orbitals *h* and *l*, which stand for HOMO and LUMO. The distribution of two electrons in these two spatial orbitals, i.e., four spin orbitals, result in three singlet states (S_{0-2}) and one triplet state (T_1). The energies of these states can be exactly expressed as functions of the HOMO-LUMO gap (Δ_{hl}), the exchange integral (K_{ab}) between localized orbitals *a* and *b*, and the exchange integral (K_{hl}) between HOMO and LUMO[19,20].

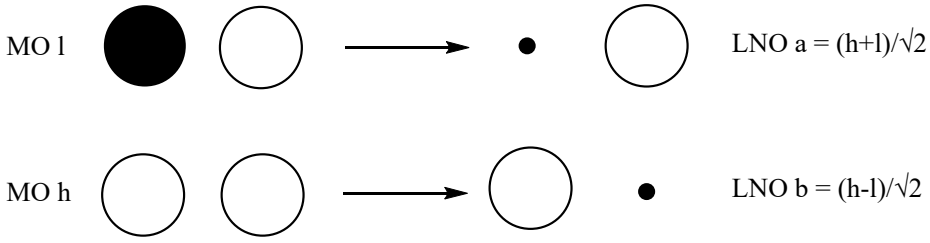

Figure 2: Schematic of the two-site model, with two electrons in two orbitals, comparing the bonding and antibonding molecular orbitals to the localized natural orbitals

Using E(S_0) as the 0 reference, the excitation energies read:

$$E(T_1) = -K_{hl} - 2K_{ab} + \sqrt{K_{hl}^2 + \Delta_{hl}^2} \quad Eq.(4)$$

$$E(S_1) = K_{hl} - 2K_{ab} + \sqrt{K_{hl}^2 + \Delta_{hl}^2} \quad Eq.(5)$$

These two excited states are expressed using the Slater determinants of the localized orbitals *a* and *b* and the delocalized canonical orbitals *h* and *l* as:

$$|T_1\rangle = |ab\rangle = |hl\rangle \quad Eq.(6)$$

$$|S_1\rangle = \frac{1}{\sqrt{2}}\left(|a\bar{a}\rangle - |b\bar{b}\rangle = \frac{1}{\sqrt{2}}\left(|h\bar{l}\rangle - |\bar{h}l\rangle\right)\right) \quad Eq.(7)$$

Here, $|ab\rangle$, $|h\bar{l}\rangle$, etc. are Slater determinants of spin orbitals. The overhead bar denotes spin orbitals with β spin. The spin orbitals without the overhead bar are with the α spin. Please note that the HOMO-to-LUMO triplet excitation is a pure diradical state in the localized orbitals representation, while the HOMO-to-LUMO singlet excitation gives a charge-transfer state in the localized representation, with both electrons on the spatial orbital *a*, or on the spatial orbital *b*.

The diradical character at the ground state is indicated by

$$y_0 = 1 - \frac{1}{\sqrt{1 + \left(\frac{K_{hl}}{\Delta_{hl}}\right)^2}} \quad Eq.(8)$$

Clearly, the diradical character is solely determined by the $\frac{K_{hl}}{\Delta_{hl}}$ ratio, not separately by K_{hl} and Δ_{hl}. The increase of K_{hl} and the decrease of Δ_{hl} enhance the diradical character. The following ratios can be expressed using y_0:

$$\frac{\Delta_{hl}}{\sqrt{K_{hl}^2+\Delta_{hl}^2}} = 1-y_0; \frac{K_{hl}}{\sqrt{K_{hl}^2+\Delta_{hl}^2}} = \sqrt{1-(1-y_0)^2} \quad Eq.(9)$$

Then we have

$$\sqrt{K_{hl}^2+\Delta_{hl}^2} = \frac{K_{hl}}{\sqrt{1-(1-y_0)^2}} \quad Eq.(10)$$

Using this expression of $\sqrt{K_{hl}^2+\Delta_{hl}^2}$, the excitation energies are expressed as

$$E(T_1) = -K_{hl} - 2K_{ab} + \frac{K_{hl}}{\sqrt{1-(1-y_0)^2}} \quad Eq.(11)$$

$$E(S_1) = K_{hl} - 2K_{ab} + \frac{K_{hl}}{\sqrt{1-(1-y_0)^2}} \quad Eq.(12)$$

Then,

$$2E(T_1) - E(S_1) = -3K_{hl} - 2K_{ab} + \frac{K_{hl}}{\sqrt{1-(1-y_0)^2}}, \quad Eq.(13)$$

which is renormalized by $2K_{hl}$ to be

$$f = \frac{2E(T_1)-E(S_1)}{2K_{hl}} = -\frac{3}{2} - \frac{K_{ab}}{K_{hl}} + \frac{1}{2\sqrt{1-(1-y_0)^2}} \quad Eq.(14)$$

This equation shows that the dimensionless variable *f*, which governs the satisfaction of Eq. (1), is dependent on y_0 and the K_{ab}/K_{hl} ratio[21].

A larger y_0 is desired for $2E(T_1) - E(S_1)$, and so is a larger $\frac{K_{ab}}{K_{hl}}$. **Figure 3**(a) shows that y_0 plays a larger role in determining the sign of *f*, since for the four examined $\frac{K_{ab}}{K_{hl}}$ quantities, the *f*

curves cross the zero value at similar y_0 values. Since y_0 is determined by $\frac{K_{hl}}{\Delta_{hl}}$, it is desirable to see how K_{hl} and Δ_{hl} affect $E(T_1)$ and $E(S_1)$.

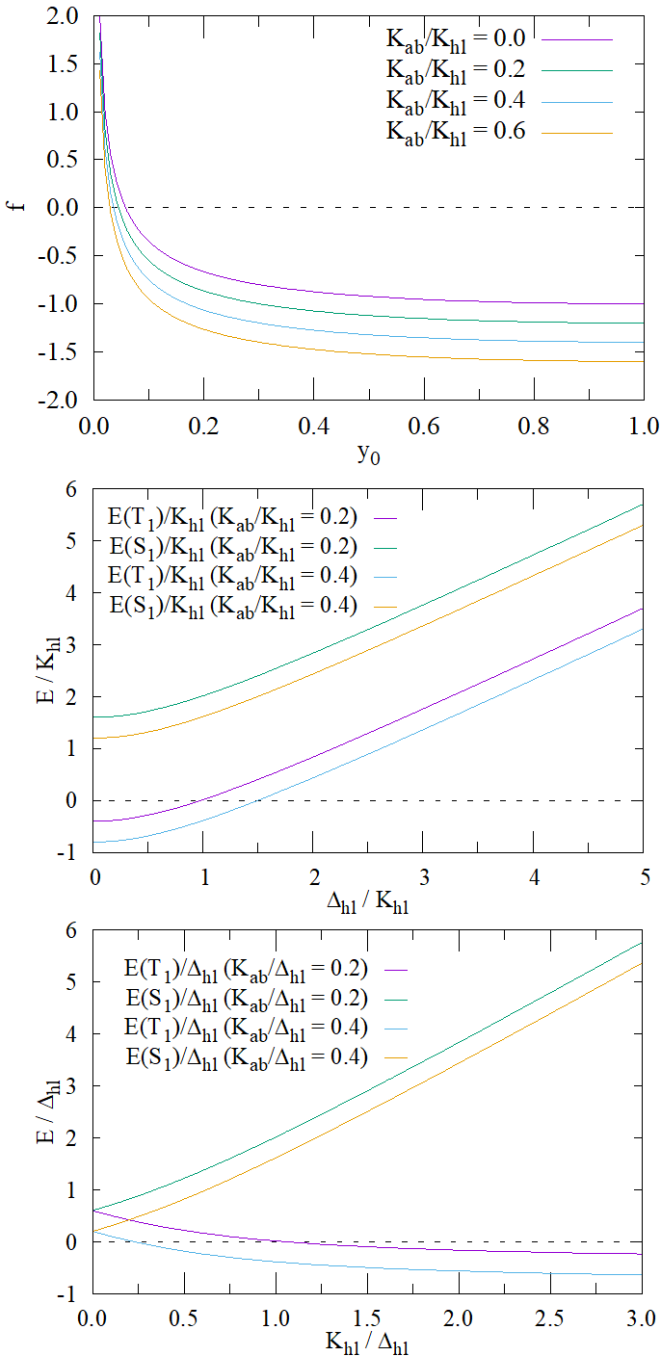

Figure 3: (a) Variation of f as a function of diradical character (y_0) and the K_{ab}/K_{hl} ratio, (b) variation of $E(S_1)$ and $E(T_1)$ as functions of Δ_{hl}, while K_{hl} is fixed, and (c) variation of $E(S_1)$ and $E(T_1)$ as functions of K_{hl}, while Δ_{hl} is fixed.

Plotted in **Figure 3**(b) are the variations of the two excitation energies as functions of Δ_{hl}, with a constant K_{hl}. Clearly, E(S_1) and E(T_1) decrease in a parallel fashion as Δ_{hl} decreases. But the decrease in E(T_1) counts twice in 2E(T_1) – E(S_1), such a Δ_{hl}-driven increase of y_0 still facilitates the sign change of f from positive to negative. Plotted in **Figure 3**(c) are the variations of the two excitation energies as functions of K_{hl}, with a constant Δ_{hl}. On the increase of K_{hl}, E(S_1) increases while E(T_1) decreases. The opposite trends of the two energies favor a negative sign of f when K_{hl} increases.

Back to **Figure 3**(a), we see that a not too large y_0, say around 0.1, is enough to have a negative f, i.e., satisfying Eq. (1). This result is inspiring. We may start with a conventional closed-shell system with essentially no diradical character, and then slightly enhance its diradical character by introducing substitutions, so that the modified system satisfies Eq. (1).

We need to note that the two sites model, with two electrons in two orbitals, only provides a qualitative description of the low-lying states. Actual electronic states are more complicated, and their energies do not follow the clean and simple expressions given above. However, the qualitative model does provide a clear guidance on designing SF chromophores, by connecting the fine relations between excitation energies to chemists' instinct on enhancing diradical character of molecules.

The connection between diradical character in the ground state and the satisfaction of Eq. (1) can be explained in plain language as follows. The T_1 state is a pure diradical state, with one electron in the HOMO, and the other in the LUMO. If there is sufficient diradical character in the S_0 state, meaning that there is a partial promotion from the HOMO electron pair to the LUMO, it is easier overall for the molecule's electronic structure to rearrange into the T_1 state. This easiness indicates that sufficient diradical character in the ground state is correlated with a low E(T_1) and

the subsequent satisfaction of the $E(S_1) > 2E(T_1)$ requirement. On the other hand, having too much diradical character and a too low $E(T_1)$ is detrimental, since it means high reactivity and instability of a molecule. Therefore, a molecule with an appropriate diradical character, not too little yet not too much, can be a candidate SF chromophore. The T_2 state, while higher in energy than the T_1 state, may also be affected by diradical character in the S_0 state. If the frontier orbitals involved in ground state diradical character extend beyond the typical HOMO⇒LUMO occupancy e.g., it consists of substantial HOMO-1⇒LUMO+1 promotion or HOMO⇒LUMO+1 promotion, then the S_0 state can be thought of as having multiple diradical character. The ⇒ symbol indicates two-electron promotion due to electron correlation, while the → symbol indicates one-electron transfer due to excitation. In this state, the electronic rearrangement to T_2 is easier, and hence, a low-lying T_2 state results. It is clear then, that the requirement of $E(T_2) > 2E(T_1)$ is highly correlated with a molecule's second fold of diradical character, i.e., tetraradical character.

1.4: Molecular Design

The selective conditions of having not too little yet not too much diradical character and little tetraradical character determines the fact that only a handful of molecules undergo SF. This fact motivates our present work in designing SF chromophores using computational chemistry. Starting with pristine parent structures, it is possible to tune the diradical character to desirable levels through the introduction of substituents.

Traditional design approaches utilizing the captodative effect[22-29] and the (anti)aromaticity[18,30-34] to enhance diradical character have proven to be effective. This thesis reports on a new strategy of substitution for the design of singlet fission chromophores. Aromatic systems show enhanced stability when compared to nonaromatic systems. They also have good

absorption of electromagnetic radiation. They are hence natural parent structures for designing SF chromophores. Aromatic systems, despite their stability, may feature some diradical character in their ground states. One example of anthracene is shown in **Figure 4**. Anthracene can take the closed-shell resonance structure on the left, which has one aromatic sextet at the central ring and two butadienyl fragments on the two side rings, or the closed-shell resonance structure at the middle, which has an aromatic sextet on one side ring and then an *o*-quinodimethanyl fragment in the rest, and the left-right symmetry image of this structure. It can also take the diradical resonance structure on the right, which has two aromatic sextets on the two side rings and two radical sites at the center. The diradical structure plays a role in the anthracene ground state because of its larger number of aromatic sextets[35], which counterpoise the instability induced by having two radical sites.

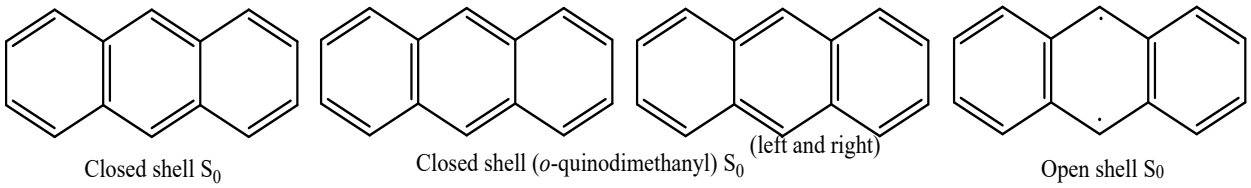

Figure 4: The four resonance structures of anthracene: the closed-shell structure with a central sextet and two butadienyl fragments on the two sides (left), the closed-shell structures with a side sextet and an *o*-quinodimethanyl fragment (the two middle ones), and the diradical structure with two aromatic sextets (right).

If we can stabilize the resonance structure by introducing substitutions, we can enhance the diradical character of the molecule and design SF chromophores that satisfy Eq. (1). The strong π interactions between the sp^2 C atoms disfavor the diradical resonance structure in **Figure 4**, despite its nonzero contribution to the ground state. Therefore, substitutions of the two radical C atoms with radical stabilizing moieties, which participate less in the π interactions, will enhance the

diradical character of the molecule. On the other hand, the substitutions should maintain the 4n+2 aromatic stability.

In this thesis, the pristine parent structure and radical moiety were chosen to be anthracene and N-oxyl respectively. Anthracene itself was chosen as historically SF was first observed in anthracene through the delayed fluorescence in its crystal[3]. Anthracene, however, does not satisfy the $E(S_1) > 2E(T_1)$ requirement, and as such, it experiences at best an endoergic, slow singlet fission. Anthracene has the benefit of being smaller than more extensively investigated SF chromophores like tetracene and pentacene. Small chromophores are desired because they facilitate the development of light-weighted mini OPV devices with high energy density. Anthracene is also easily isolated from coal sources[36,37]. The radical substituent, N-oxyl, was chosen due to its proven stability within other documented radical structures such as tetramethylpiperidine N-oxyl (TEMPO) and phthalimide N-oxyl (PINO)[38].

The stability of the NO-containing radical fragment arises from the following aspects. (1) The NO-centered radical fragment can be seen as isoelectronic and isosteric to an acyl anion. The unpaired electron resides in the NO π^* orbital. The large electronegativities of N and O (vs C) stabilize the antibonding orbital and hence mitigate the reactivity of the radical. Our unrestricted B3LYP/cc-pVDZ density functional theory (DFT) calculation shows that the energy of the singly occupied molecular orbital (SOMO) of the H_2NO radical is -0.212 E_H, compared to the -0.227 E_H of the methyl SOMO. The anti-bonding NO π^* orbital has only a slightly higher energy than the methyl nonbonding orbital, reflecting the stability brought by the electronegative N and O atoms.

(2) The stability of the NO radical is also favored by the NO π bonding orbitals. When the NO SOMO attempts a bonding interaction with another radical species, a mixing occurs between the NO π^* SOMO and the NO π orbital, providing an increased SOMO amplitude on the bonding

atom (either Nitrogen or Oxygen). This mixing is a destabilizing factor to the NO π bonding, and as such, provides an argument against forming a bond with another radical species. A pictorial description for such a π-π^* mixing is given in **Figure 5**. Clearly, the partial NO π bond, with two electrons in the π bonding orbital and one electron in the π^* anti-bonding orbital, is broken when the two orbitals are recombined to localized lobes on the two atoms. This breaking of a partial π bond suppresses the radical reactivity of the NO fragment.

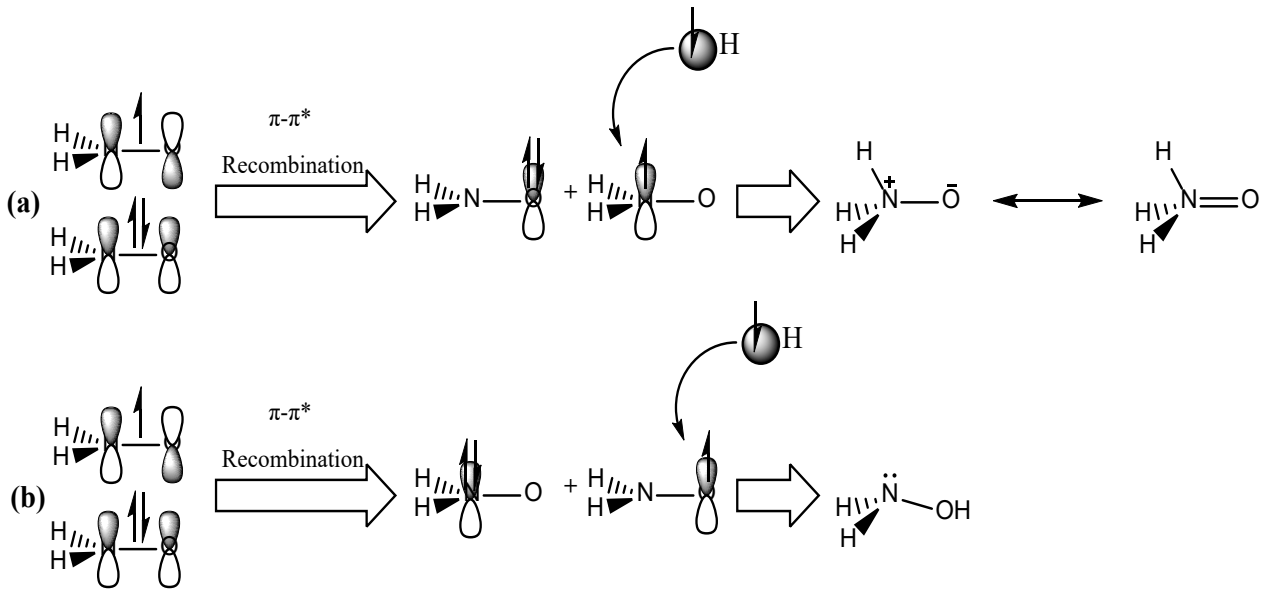

Figure 5: NO π and π^* mixing in preparation for forming a bond with an incoming H atom attacking (a) the N and (b) the O atom.

One NO fragment is a stable radical moiety, If we introduce two NO fragments in a closed-shell parent structure, we shall be able to enhance diradical character of the substituted system. In this work, all 15-di-nitro-doped anthracene structures are examined for their SF efficacy. With the right substituent placement, the molecule can likely be pushed to satisfy Eqs. (1) and (2).

Chapter 2: Computational Methods

Structural reorganization occurs rapidly after vertical excitation on a timescale that may even outcompete singlet fission. It makes sense therefore to consider the 0-to-0 $E(S_1)$, $E(T_1)$, and $E(T_2)$ as opposed to the vertical excitation energies when considering the thermodynamic requirements. "0-to-0 excitation energy" means the energy difference between the optimized structures of the ground and excited state of interest, and this energy difference is corrected by the zero-point vibrational energies of the two states at their respective optimized structures. Density functional theory (DFT) was used to optimize the S_0 and T_1 states while time-dependent density functional theory was used to optimize the S_1 and T_2 states. The B3LYP functional was used in those calculations[39,40]. Hessian calculations at the optimized structures were done at the same levels. The correlation-consistent polarized valence only double zeta (cc-pVDZ) basis set is used in the optimization and Hessian calculations[41]. At the optimized structures, single-point calculations of the excitation energies were done at the n-electron valence state perturbation theory (NEVPT2)[42-44] level using the cc-pVTZ[41] (the triple zeta analogue of the aforementioned cc-pVDZ) basis set. The NEVPT2 calculations treat both dynamical and non-dynamical electron correlations satisfactorily. Both types of correlations play significant roles in excited states. The zero-point energies (ZPE) calculated at the DFT and TDDFT levels above were added to correct the NEVPT2 single-point energies. A ten-electrons-in-ten-π-orbitals active space was used in each of the NEVPT2 calculations. The ZPE-corrected excitation energies are used to determine whether the molecules satisfy Eqs. (1) and (2). The molecules that satisfied Eq. (1) had their T_2 energies calculated. The computational methods chosen are reliable as the 2.46 eV vertical $E(S_1)$ (see Results and Discussion) of the N9N10 molecule (see the next paragraph for the notation of the investigated molecules) is consistent with the absorption spectrum peak at 490 nm (2.53 eV,

only 0.07 eV off) of this molecule[45]. The DFT and TDDFT calculations were done using the GAMESS-US[46,47] program package, while ORCA[48] was used for the NEVPT2 calculations.

The anthracene positionings are shown in scheme 1 below to facilitate subsequent discussions. We used "N1N2" to label the structure with two NO fragments replacing the two CH moieties at the C1 and C2 positions. The same logic is followed for labeling other di-NO-substituted anthracenes.

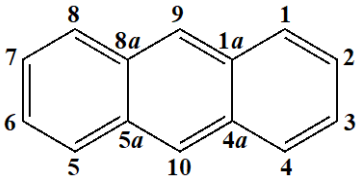

Scheme 1: Position numbering of anthracene

Chapter 3: Results and Discussion

3.1: Quantitative Evidence for the Reduced Radical Reactivity of N-Oxyl

To confirm the conjecture discussed earlier that the NO fragment is a less reactive radical system, we calculated its reaction energy with a H atom. One would expect the reaction to be significantly exothermic upon covalent bond formation between two radical species. At the B3LYP/cc-pVDZ level of theory, the reaction energy for Hydrogen addition to the N and O site of H_2NO was found to be -1.71 eV and -2.75 eV respectively. When comparing these values to Hydrogen addition on a CH_3 radical, which has a reaction energy of -4.37 eV, it is clear that the NO fragment has a less tendency to form a covalent bond with an incoming radical species, proving its relative stability. Both resonance structures of H_3NO in **Figure 5**(a) are less stable than the resonance structure of H_2NOH in **Figure 5**(b). The first H_3NO resonance structure has attendant charges on adjacent N and O atoms while the second structure does not obey the octet rule. Unlike its heavier congener Phosphorus, Nitrogen is not a typical atom that forms hypervalent molecules. Correspondingly, the H addition to O is more favorable than the addition to N by about 1 eV.

The introduction of N-oxyl into the anthracene framework implies the formation of N=N and/or N=C double bonds. It is necessary to examine the tendency of the NO radical moiety to form the π bonds. **Figure 6** shows the comparative bond energies of N=N, N=C, and C=C double bonds concerning torsional strain about their dihedral angles. **Figure 6** indicates that the C=C π bond is the strongest, followed by the N=C π bond and subsequently the N=N π bond. The weaker N=C π bond reflects the stability of the NO radical fragment and its less tendency to form a π bonding interaction with an adjacent sp^2 C atom. The even weaker N=N π bond naturally arises

when two less reactive NO radical fragments are placed adjacent to each other. The demonstrated weak π covalent interaction between the NO fragment and its neighbouring sp^2 centers is strongly desired for enhancing diradical character in the di-NO-substituted anthracenes.

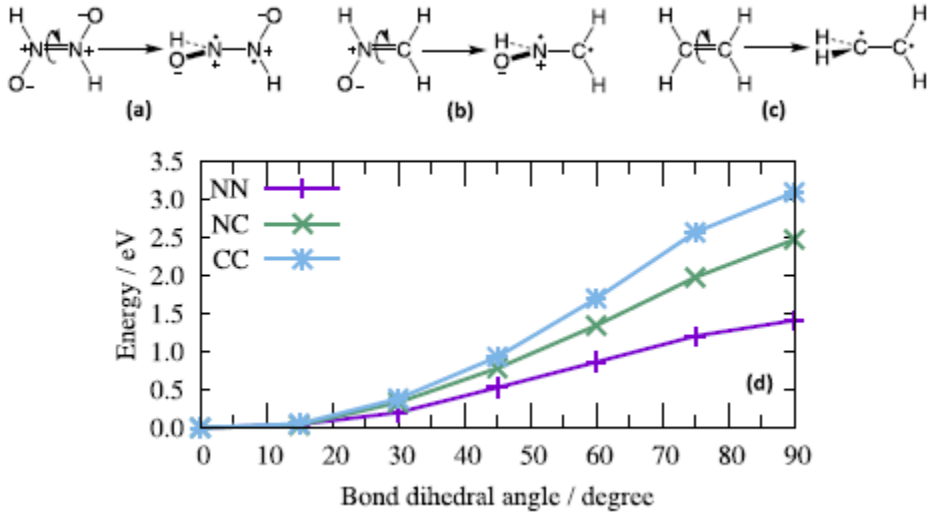

Figure 6: (a)-(c) The three structures used to show π interaction strength of the NO radical moiety. (d) The potential energy curves of the double bond rotations shown in (a)-(c). Adapted from *J. Chem. Phys.* 2022, *156*, 034303, copyright 2022 American Institute of Physics.

3.2: Diradical Character and Structural Reorganization Matter

There are in total 15 di-NO-substituted anthracenes. Plotted in **Figure 7**(a) are vertical and 0-to-0 $E(S_1)$s and $E(T_1)$s against the n_{LUNO}s for the 15 molecules. n_{LUNO} is the natural occupancy of the lowest unoccupied natural orbital and it can be used as a diradical character indicator. In this thesis, we defined

$$\Delta E_{SF}^{(1)} = E(S1) - 2E(T1) \quad Eq.(15)$$

$$\Delta E_{SF}^{(2)} = E(T2) - 2E(T1) \quad Eq.(16)$$

to quantify the extends to which the molecules satisfy Eqs. (1) and (2). Certainly, the two quantities being positive is desired. These two quantities of the 15 molecules, calculated using both vertical and 0-to-0 excitation energies, are also plotted against n_{LUNO}s in **Figure 7**(b) and (c). There are eight purple markers above the zero line in **Figure 7**(b), meaning that 8 of the 15 di-NO-substituted anthracenes satisfy Eq. (1) with their 0-to-0 excitation energies. There are six purple markers in **Figure 7**(c) above the zero line, and they all fall within the eight molecules that satisfy Eq. (1). Overall, 6 of the 15 investigated molecules satisfy Eqs. (1) and (2) with their 0-to-0 excitation energies. If our purpose is just to pick those that satisfy the two criteria, this thesis may conclude here. However, it is more important to understand why introducing the two NO radical fragments only at certain positions can lead to the desired relations between excitation energies. The knowledge will be useful for future studies in designing SF chromophores using the N-oxyl strategy.

In **Figure 7**(a), the $E(T_1)$ values, especially the vertical $E(T_1)$ values, exhibit an obvious anti-correlation with the n_{LUNO} values. Since the n_{LUNO}s were obtained at the S_0 structures of the molecules, it is not unexpected that a better anti-correlation is observed between the vertical $E(T_1)$s

and the n_{LUNO}s than between the 0-to-0 E(T_1)s and the n_{LUNO}s [the green markers vs. the purple markers in **Figure 7**(a)]. The E(S_1)s also show a trend of decrease as n_{LUNO} increases. This trend suggests that the diradical character increases mostly due to the HOMO-LUMO gap reduction (see the discussion about **Figure 3** above). The T_1 and S_1 states of all the molecules (except N1N9, see below) mainly consists of HOMO-to-LUMO one-electron excitation, so that both E(T_1) and E(S_1) decrease as the HOMO-LUMO gap decrease.

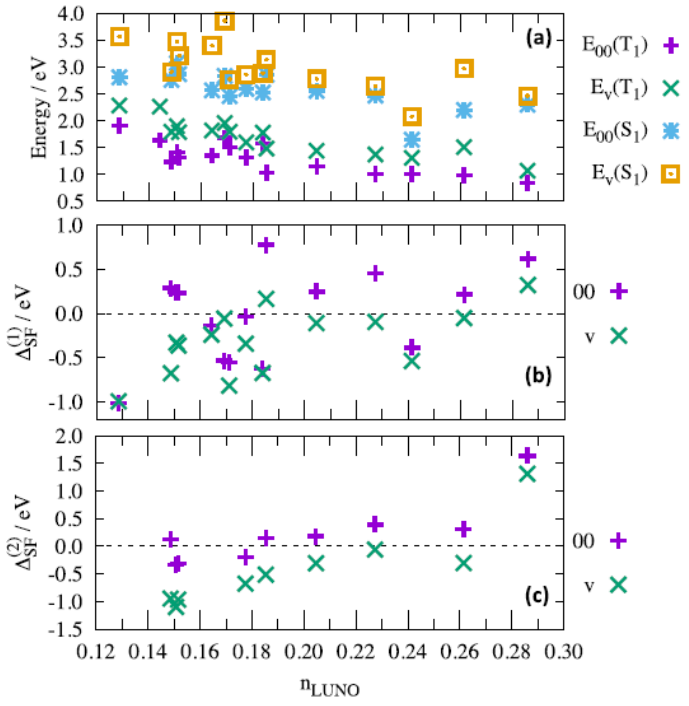

Figure 7: Plottings of (a) E(T_1), E(S_1), (b) $\Delta_{SF}^{(1)}$, and (c) $\Delta_{SF}^{(2)}$ against n_{LUNO} for the 15 investigated di-NO-substituted anthracenes. The 00 and v subscripts in (a) indicate the 0-to-0 and vertical excitation energies. The two sets of Δ_{SF} data in each of (b) and (c) are obtained using the 00 and vertical sets of E(S_1)s, E(T_2)s, and E(T_1)s. Adapted from *J. Chem. Phys.* 2022, *156*, 034303, copyright 2022 American Institute of Physics.

When only considering vertical excitation energies, only two green markers in **Figure 7**(b) are above the dashed zero line. When we consider the structural reorganization energies, labeled as $\lambda(S_1)$ and $\lambda(T_1)$, more chromophores make it over the threshold. **Figure 7**(c) shows the same effect, where the 0-to-0 excitation pushes an additional 5 chromophores over the $\Delta_{SF}^{(2)} = 0$ threshold. This evidence shines a light on the importance of structural reorganization when designing singlet fission chromophores. All relevant structural reorganization energies are summarized in **Table 1**. The reorganization energies increase $\Delta_{SF}^{(1)}$ and $\Delta_{SF}^{(2)}$ because $\lambda(T_1)$ counts twice in Eqs. (1) and (2), while $\lambda(S_1)$ and $\lambda(T_2)$ count once. The importance of considering structural reorganizations of the excited sates in judging SF propensity of a candidate chromophore is evident.

Table 1: S_1 and T_1 reorganization energies (in eV) for all 15 di-NO-substituted anthracenes

Chromophore	$\lambda(S_1)$	$\lambda(T_1)$
N2N3	**0.76**	**0.37**
N2N6	**0.34**	**0.20**
N1N3	**0.31**	**0.29**
N2N7	**0.51**	**0.28**
N1N9	**0.38**	**0.29**
N1N7	**0.83**	**0.47**
N2N10	**0.26**	**0.28**
N1N8	**0.34**	**0.47**
N1N6	**0.40**	**0.48**
N1N2	**0.77**	**0.52**
N2N9	**0.22**	**0.29**
N1N5	**0.15**	**0.56**
N1N4	**0.18**	**0.36**
N9N10	**0.17**	**0.23**
N1N10	**0.28**	**0.44**

Of the 15 di-nitro substituted anthracenes, 6 did not satisfy Eq. (1), 3 satisfied Eq. (1) but not Eq. (2), and 6 satisfied both, which are the singlet fission chromophore candidates. In the following three subsections, we discuss these three groups of structures respectively, with the

objective to purpose a general guideline for future studies in designing SF chromophores through similar strategies of introducing radical fragments in closed-shell pristine structures.

3.3: The 6 Molecules that did not Satisfy $E(S_1) > 2E(T_1)$

The calculated energies and natural occupancies of the six molecules that do not satisfy Eq. (1) are summarized in **Table 2**. N1N9 is of special interest among the six. Surprisingly, its 0.241 large n_{LUNO} does not make it satisfy Eq. (1). The diradical character arises from electron correlation that promotes the HOMO electron pair to LUMO in S_0. The highest occupied natural orbital (HONO) and lowest unoccupied natural orbitals (LUNO) of N1N9 are shown in **Figure 8**(b) and (c). They resemble the HOMO and LUMO. Henceforth, we use natural orbitals to discuss wavefunctions of the molecules. They resemble canonical MO's, and they better represent wavefunctions, as configuration interaction wavefunctions take the shortest expansions if natural orbitals are used. The HONO and LUNO exhibit NO π^* character and have large amplitudes on C4 and C10, which are para to the Nitrogen atoms. The two natural orbitals suggest a resonance of diradical structures shown in **Figure 8**(d). The T_1 state of this molecule involves HONO→LUNO (abbreviated as H→L) excitation and adopts the resonance structures in **Figure 8**(f). The large n_{LUNO} is consistent with the 1.02 eV low $E(T_1)$ of the molecule. **Figure 7**(a) shows a dip in the two sets of $E(S_1)$ data at n_{LUNO} =0.241. It is the low $E(S_1)$, rather than a high $E(T_1)$, that makes the negative Δ_{SF}^1.

The S_1 state of N1N9, at both its S_0 and S_1 structures, arises from H-5→L excitation. The HONO-5 is shown in **Figure 8**(a). The H→L excitation generates S_2, whose vertical excitation energy is 0.61 eV above S_1. The low energy H-5→L excitation arises from: (1) the hole and electron orbitals (HONO-5 and LUNO) have small spatial overlap, so that the charge transfer

energy in this singlet excitation is low; (2) the antibonding interaction in HONO-5 between the in-plane O lone pair orbitals is relieved in this excitation. N1N9 has the shortest OO distance (r_{OO}) among all the studied molecules and is the only one that features such a strong OO antibonding interaction. The structural parameters of the S_1 optimized structure are shown in **Figure 8**(e). r_{OO} is significantly reduced from 2.54 Å in the S_0 structure to 2.16 Å in the S_1 structure, due to the reduction in the OO antibonding interaction by this excitation. The S_1 resonance structures in **Figure 8**(e) are assigned based on the distributions of HONO-5 and LUNO. Overall, the failure of N1N9 as a SF chromophore is not because of low diradical character, but the σ^* interaction between two O atoms in close contact. A 12 electrons in 11 orbitals active space was employed in all NEVPT2 calculations for N1N9, with the additional in-plane HONO-5.

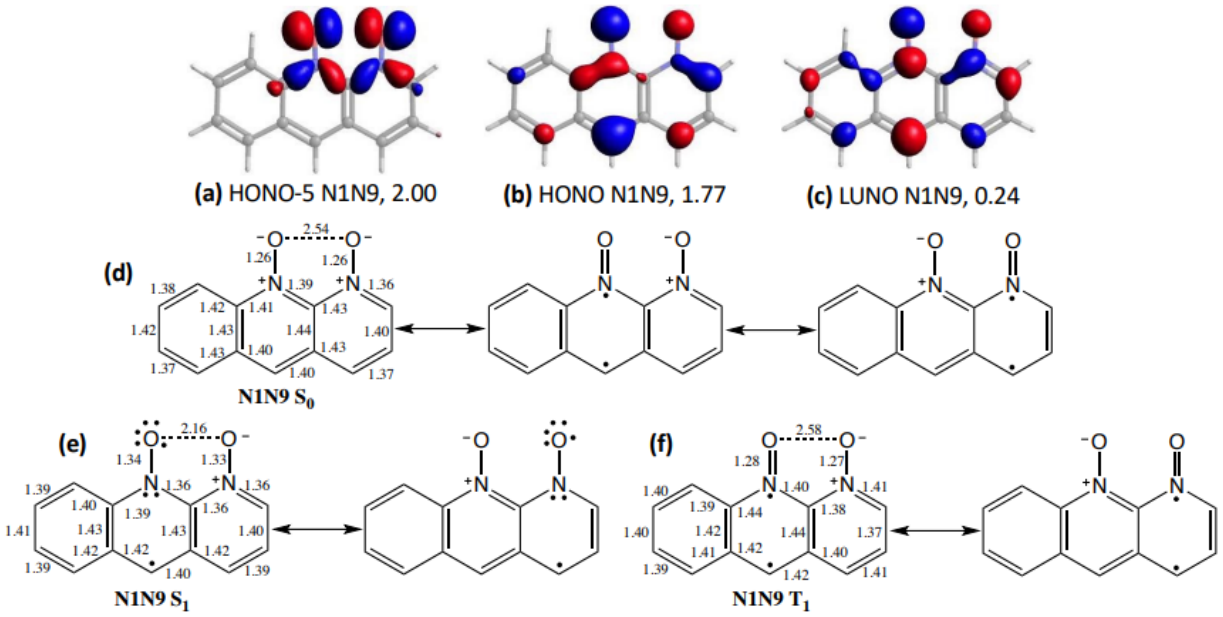

Figure 8:Frontier natural orbitals involved in S_1 and T_1 excitations of N1N9; bond lengths (in Å) and resonance structures of S_0, S_1, and T_1 of N1N9. Occupancies of the natural orbitals are given under their plottings. Adapted from *J. Chem. Phys.* 2022, *156*, 034303, copyright 2022 American Institute of Physics.

Table 2:Energy values for the first singlet excited state, the first triplet excited state, the energy level matching condition E(S1)-2E(T1)/ΔE_{SF}^{1}), and natural orbital occupations of LUNO and LUNO+1. All energy values are reported in the units of eV.

Chromophore	$E(S_1)$	$E(T_1)$	$E(S_1)-2E(T_1)$ $[\Delta E_{SF}^{(1)}]$	n_{LUNO}	n_{LUNO+1}
N2N3	**2.81**	**1.91**	**-1.01**	**0.129**	**0.113**
N1N3	**2.46**	**1.50**	**-0.55**	**0.171**	**0.097**
N2N6	**2.53**	**1.58**	**-0.63**	**0.184**	**0.109**
N2N7	**2.83**	**1.68**	**-0.54**	**0.169**	**0.132**
N1N7	**2.57**	**1.35**	**-0.14**	**0.164**	**0.112**
N1N9	**1.65**	**1.02**	**-0.39**	**0.241**	**0.113**

The other 5 molecules discussed in this subsection fall in the low to relatively low n_{LUNO} region in **Figure 7**(b) and feature relatively high $E(T_1)$s. N2N3 has the lowest n_{LUNO} = 0.129 amongst all molecules considered in this work, even lower than the 0.144 n_{LUNO} of the pristine anthracene. The HONO-1 to LUNO+1 of N2N3 are shown in **Figure 9**(a)-(d). Their distributions and the almost degenerate occupancies of HONO-1 and HONO, and of LUNO and LUNO+1 indicate two CN π fragments at the side ring. If we force the NO moieties to be radical centers, the leftover C fragment must adopt a diradical structure of 2,3-naphthoquinodimethane (**Figure 9**(e)), since the naphthalenyl moiety of the left and central rings would like to maintain its aromaticity. The four adjacent radical centers must interact strongly to give the S_0 state with little diradical character, but some tetraradical character from the two CN π bonds. The adjacent N centers adopt +1 attendant charges in the closed-shell Lewis structure in **Figure 9**(e). Their coulomb repulsion leads to the exceptionally long r_{NN} = 1.65 Å. With the low diradical character, N2N3 has a 1.91 eV high $E(T_1)$ and the most negative $\Delta_{SF}^{(1)}$ = -1.01 eV in the present thesis.

A similar argument applies to N1N3, whose two N centers also reside in the side ring. The two N centers are not adjacent to each other and the π interaction occurs across the four atoms in the side ring and leads to a 1,3-butadienyl-like fragment (N1C2N3C4), as shown by the HONO-1 to LUNO+1 of the molecule (**Figure 9**(f)-(i)). The diradical character of the genuine 1,3-butadiene arises from its two termini. However, only one N radical stabilizer is at the terminal position (**Figure 9**(i)). The other NO moiety at position 3 wastes its capability of stabilizing the other radical. With its relatively low diradical character, N1N3 does not satisfy Eq. (1).

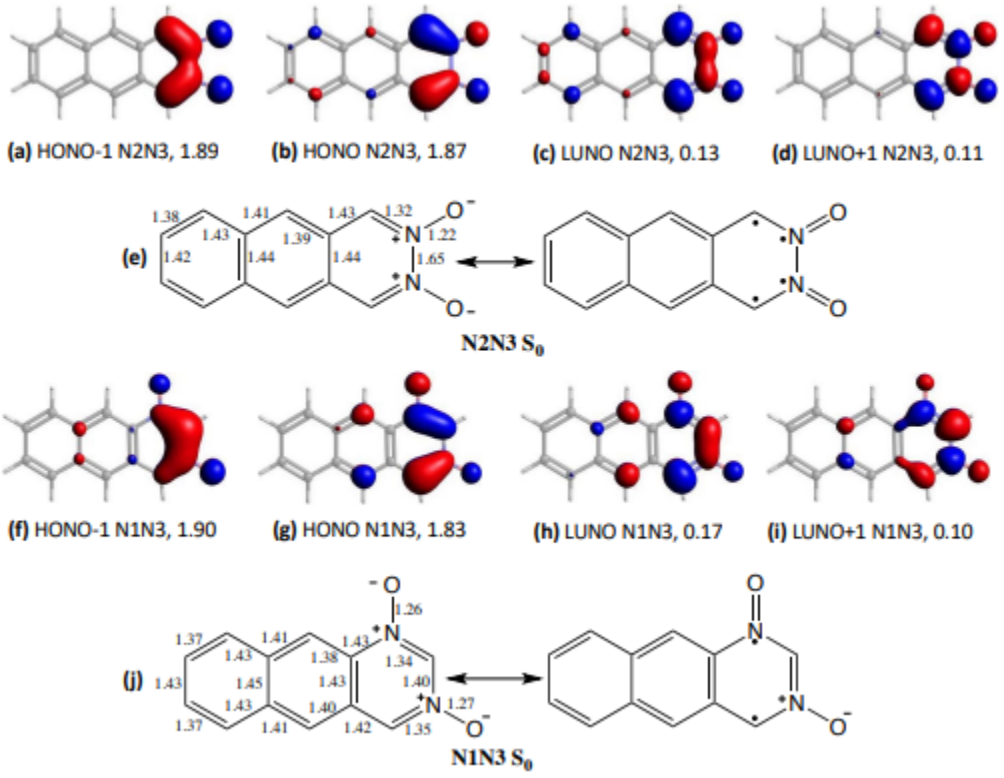

Figure 9:Frontier natural orbitals, bond lengths (in Å), and resonance structures of N2N3 and N1N3. Occupancies of the natural orbitals are given under their plottings. Adapted from *J. Chem. Phys.* 2022, *156*, 034303, copyright 2022 American Institute of Physics.

N2N6 has a fairly high E(T_1) = 1.56 eV. The HONO and LUNO of this molecule (**Figure 10**(b) and (c)) indicates diradical character on the two 1,3-butadienyl-like fragments

(**Figure 10**(e)), N2C1C1*a*C9 and N6C5C5*a*C10. The HONO-1 and LUNO+1 (**Figure 10**(a) and (d)) indicate the tetraradical character on the two C1N2 and C5N6 π bonds. Each of the NO moieties only contributes to one of the 1,3-butadienyl-like fragments and exerts limited stabilization of the two diradical resonance structures. The 0.184 n_{LUNO} can be viewed as an addition of the two fragments' diradical characters, while each of the fragments has only limited diradical character. Correspondingly, the excitation to T_1, which is a linear combination of the triplet excitations on the 1,3-butadienyl-like fragments, involves the 1.56 eV high energy.

A similar argument applies to N2N7, whose frontier natural orbitals are shown in **Figure 10**(i)-(l). They demonstrate π and π^* characters between N and their adjacent C1 and C8. The corresponding resonance structures are shown in **Figure 10**(m). The diradical characters are contained by the separate CN π fragments. The two N centers do not synergize to enhance diradical character. This is especially so in order to maintain the central aromatic sextet, which isolates the two N radical centers on the two side rings. A 1.68 eV high $E(T_1)$ ensues. The 1.03 eV large λ (S_1) also contributes to the negative $\Delta_{SF}^{(1)}$ = -0.54 eV. λ (T_1) is just 0.28 eV. Without considering structural reorganizations, $\Delta_{SF}^{(1)}$ was calculated to be only slightly negative, -0.06 eV, using the vertical $E(S_1)$ and $E(T_1)$.

N1N7 has a similar electronic structure to N2N7, with one of the CN π fragments swapping the N and C positions. The frontier natural orbitals of N1N7 (**Figure 10** (n)-(q)) resemble the N2N7 counterparts and so do the bond lengths and resonance structures (**Figure 10** (r) vs. (m)). N1N7 hence also has a 1.82 eV high vertical $E(T_1)$, which is reduced by structural reorganization to 1.35 eV. Still, it is too high to satisfy Eq. (1).

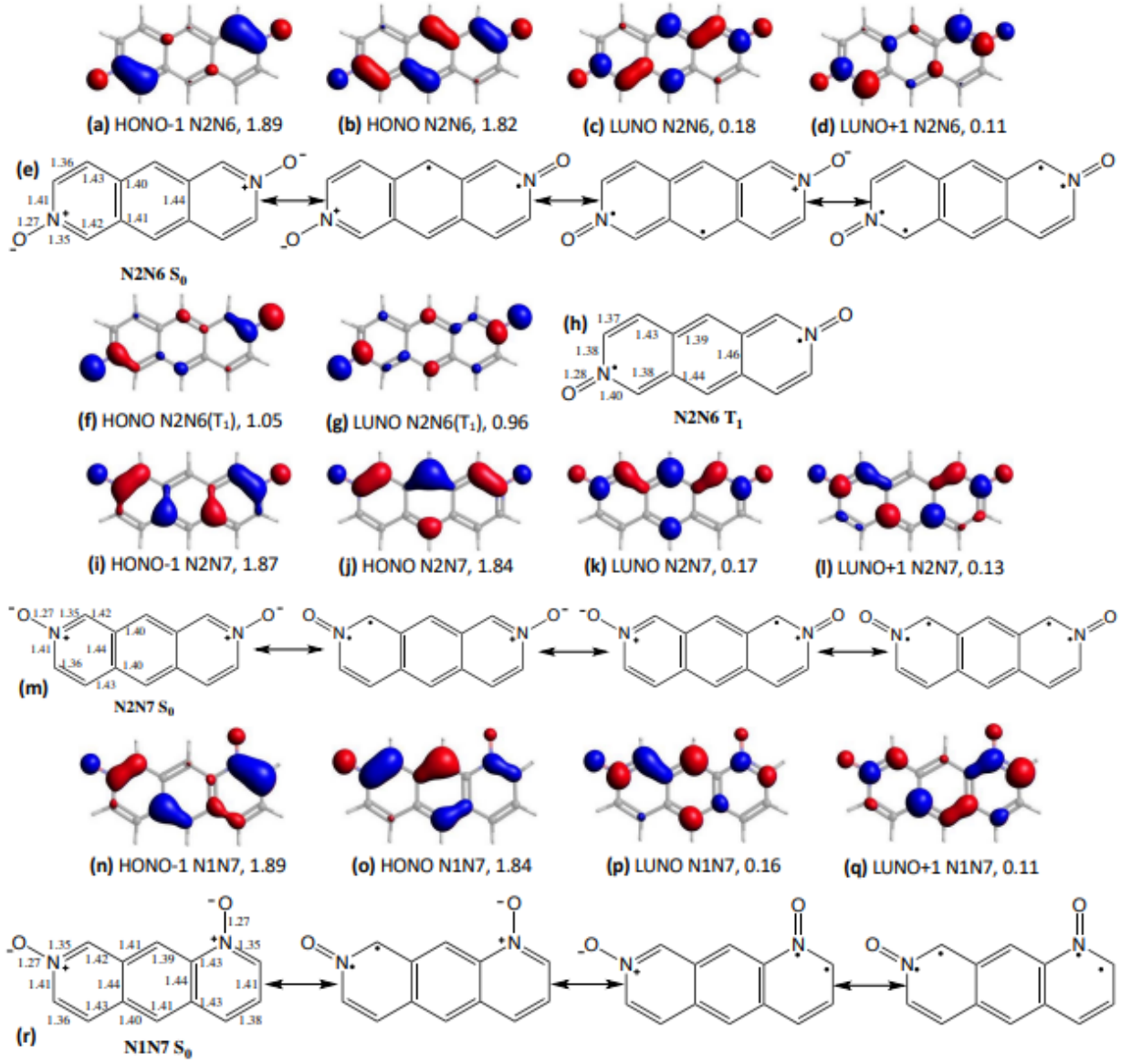

Figure 10: Frontier natural orbitals, bond lengths (in Å), and resonance structures of N2N6, N2N7, and N1N7. Occupancies of the natural orbitals are given under their plottings. "(T_1)" in (f)-(h) indicates that those orbitals and bond lengths were obtained at the T_1 optimized structure of the molecule. Adapted from *J. Chem. Phys.* 2022, *156*, 034303, copyright 2022 American Institute of Physics.

3.4: The 3 Molecules that Satisfied $E(S_1) > 2E(T_1)$ but not $E(T_2) > 2E(T_1)$

Table 3: First singlet, triplet, and second triplet excited state energies. The two energy level matching conditions $E(S_1)-2E(T_1)/\Delta E_{SF}^{(1)}$ and $E(T_2)-2(ET_1)/\Delta E_{SF}^{(2)}$ considered in this paper, and n_{LUNO}/n_{LUNO+1} occupation numbers. All energy values are reported in the units of eV.

Chromophore	$E(S_1)$	$E(T_1)$	$E(T_2)$	$E(S_1)-2E(T_1)$ $[\Delta E_{SF}^{(1)}]$	$E(T_2)-2(ET_1)$ $[\Delta E_{SF}^{(2)}]$	n_{LUNO}	n_{LUNO+1}
N2N10	**2.59**	**1.32**	**2.44**	**-0.04**	**-0.20**	**0.178**	**0.098**
N1N8	**2.87**	**1.32**	**2.33**	**0.23**	**-0.31**	**0.152**	**0.104**
N1N6	**3.07**	**1.42**	**2.51**	**0.24**	**-0.33**	**0.151**	**0.100**

N2N10, N1N8, and N1N6 are three such structures. Their calculated results are represented in **Table 3**. The slightly negative $\Delta_{SF}^{(1)}$ of N2N10 means that it essentially satisfies Eq. (1) with small thermal activation. The n_{LUNO+1}s for all 15 investigated molecules range from 0.08 to 0.13, a narrower range than the n_{LUNO} distribution from 0.13 to 0.29. Correspondingly, most of the reported $E(T_2)$s fall in a smaller range from 2.22 to 2.61 eV. It is the $E(T_1)$s which vary in a larger range from 0.84 to 1.90 eV, that to a larger extent, determine the signs of the $\Delta_{SF}^{(2)}$ values. Therefore, diradical character and $E(T_1)$ are still the focus of discussion for the sign of $\Delta_{SF}^{(2)}$. The frontier natural orbitals of N2N10 are shown in **Figure 11**(a)-(d). The HONO and LUNO point to a bis-allyl-like diradical resonance structure in **Figure 11**(e). The HONO-1 and LUNO+1 indicate another fold of diradical character in the right-side ring, with the radical centers at the N and C at positions 2 and 4*a*. The two folds of diradical character add up to give the tetraradical resonance structure in **Figure 11**(e). Only the N at position 10 contributes to stabilize the bis-allyl diradical character. The not too low 1.35 eV $E(T_1)$ leads to the slightly negative $\Delta_{SF}^{(1)}$ yet a -20 eV substantially negative $\Delta_{SF}^{(2)}$. The T_2 state of N2N10 involves HONO-1→LUNO and

HONO→LUNO+1 one-electron excitations. T_2 can be understood as a linear combination of the two diradical structures in **Figure 11**(e).

N1N8 is similar to N2N7, with both CN π fragments swapping the N and C positions. The frontier natural orbitals of the two molecules resemble each other (**Figure 11**(f)-(i) vs **Figure 10**(i)-(l)), and so do their resonance structures (**Figure 11**(j) vs. **Figure 10**(m)). However, the two molecules have very different $\Delta_{SF}^{(1)}$s, 0.23 vs -0.54 eV. Actually, if using vertical E(S_1)s and E(T_1)s, closer $\Delta_{SF}^{(1)}$s of -0.36 and -0.57 eV were obtained for N1N8 and N2N7, respectively. The 0.47 eV large λ(T_1) of N1N8 plays a decisive role in reversing the sign of the molecule's $\Delta_{SF}^{(1)}$. Along with the large reorganization energy is a pseudo-Jahn-Teller (pJT) distortion of the N1N8 T_1 state from C_{2v} symmetry to C_s symmetry. The HONO and LUNO of the T_1 state at its optimized structure are shown in **Figure 11**(k) and (l). They indicate the diradical structure shown in **Figure 11**(m). Such a pJT interaction is absent in N2N7, whose λ(T_1) is 0.28 eV, much lower than the N1N8 counterpart. Despite its large λ(T_1), N1N8 does not have a low enough E(T_1) to satisfy Eq. (2).

N1N6 can be viewed as being derived from N2N6, swapping the N and C atoms at positions 1 and 2. However, N1N6 has less diradical character (n_{LUNO} = 0.151 vs 0.184) and correspondingly a higher vertical E(T_1) (1.90 vs. 1.78 eV) than N2N6. The frontier natural orbitals of N1N6 are shown in **Figure 11**(n)-(q). Instead of the two butadienyl-like fragments in N2N6, these orbitals indicate a bis-allyl fragment in the left and central rings and a CN π fragment in the right ring (**Figure 11** (r)). Neither N center contributes to stabilize the bis-allyl diradical fragment. The satisfaction of Eq. (1) of N1N6 mainly arises from its large λ(T_1) and high E(S_1). In N2N6, the S_1 excitation can be viewed as consisting of short-distance charge transfers within the two butadienyl-fragments in **Figure 10**(e). In N1N6, S_1 consists mostly of the longer-distance charge transfer

between the upper and lower edges of the bis-allyl fragment in **Figure 11**(r). The longer distance charge transfer results in the higher E(S_1) (3.07 vs. 2.83 eV). The 0.48 eV large $\lambda(T_1)$ results in a lower 0-to-0 E(T_1) = 1.42 eV for N1N6 than the 1.58 eV of N2N6. The concentration of the diradical character on N1 and C4C4*a*C10 allyl fragment (**Figure 11**(s)-(u)) and the significant structural reorganization enhance each other. In N2N6, the T_1 excitation concentrates the diradical character on the two N centers (**Figure 10**(f)-(h)), along with a small $\lambda(T_1)$ = 0.20 eV. The small $\lambda(T_1)$ is not unexpected, since the T_1 resonance structure in **Figure 10**(h) is likely to also contribute to the S_0 state. The substantially different diradical characters in the S_0 and T_1 structures of N1N6 once again indicate the importance of moving beyond the two sites model assuming frozen frontier orbitals and considering structural reorganization in designing SF chromophores. The 1.42 eV E(T_1) is still too high for N1N6 to satisfy Eq. (2).

A common feature of the S_0 resonance structures of N2N10, N1N8, and N1N6 is that the two N centers do not synergize to stabilize one diradical fragment, but stabilize two separate diradical fragments. Therefore, the N centers enhance tetraradical character more than diradical character, explaining the failures of the three molecules to satisfy Eq. (2).

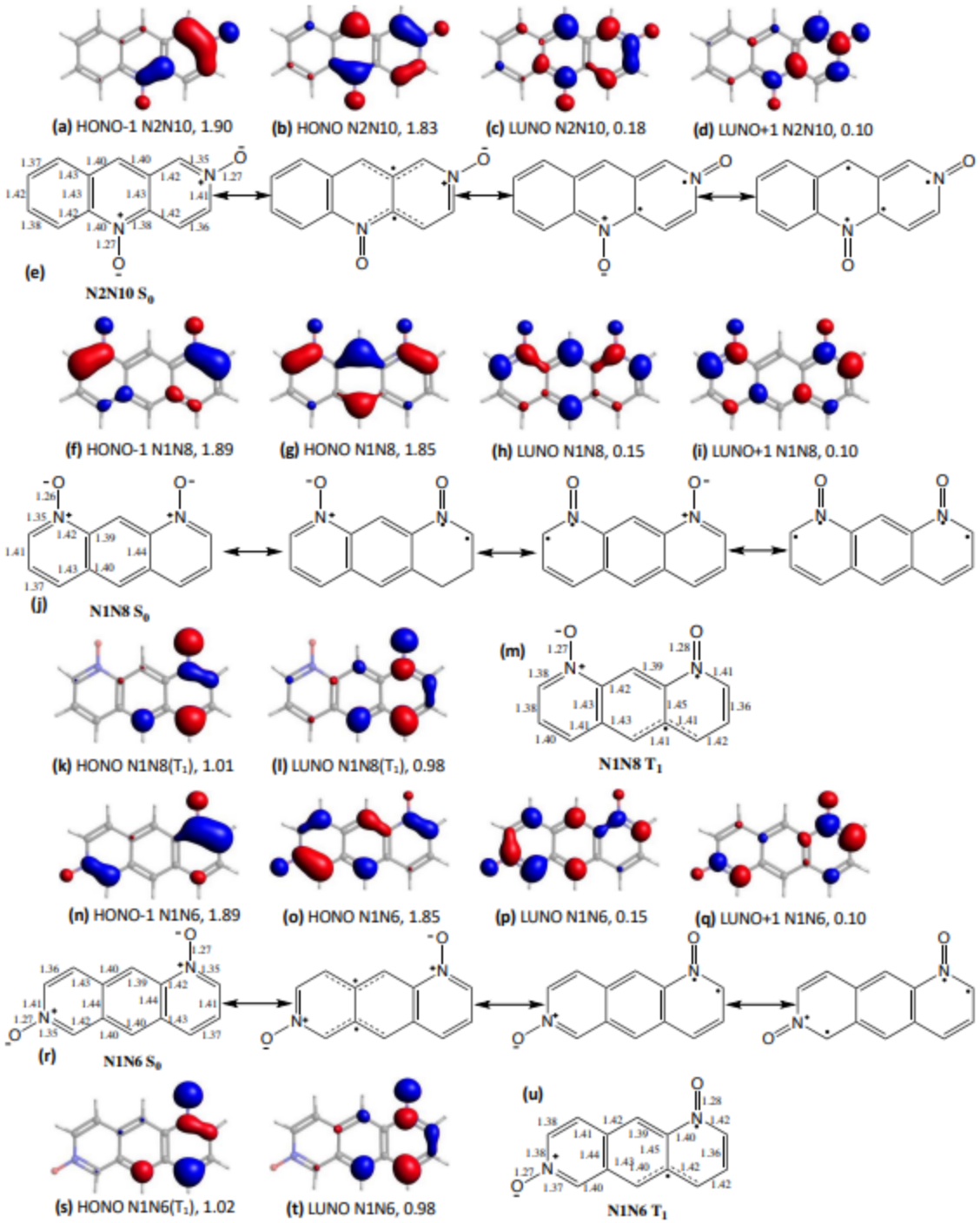

Figure 11: Frontier natural orbitals, bond lengths (in Å), and resonance structures of N2N10, N1N8, and N1N6. Occupancies of the natural orbitals are given under their plottings. "(T_1)" in (k)-(m) and (s)-(u) indicates that those orbitals and bond lengths are obtained at the T_1 optimized structures of the molecules. Adapted from *J. Chem. Phys.* 2022, *156*, 034303, copyright 2022 American Institute of Physics.

3.5: The 6 Molecules that Satisfy the Two Singlet Fission Criteria

Table 4: First singlet, triplet, and second triplet excited state energies. The two energy level matching conditions, $E(S_1)-2E(T_1)/\Delta E_{SF}^{(1)}$ and $E(T_2)-2(ET_1)]/\Delta E_{SF}^{(2)}$ considered in this paper and n_{LUNO}/n_{LUNO+1} occupation numbers. All energy values are reported in the units of eV.

Chromophore	$E(S_1)$	$E(T_1)$	$E(T_2)$	$E(S_1)-2E(T_1)$ $[\Delta E_{SF}^{(1)}]$	$E(T_2)-2(ET_1)$ $[\Delta E_{SF}^{(2)}]$	n_{LUNO}	n_{LUNO+1}
N1N2	**2.20**	**0.99**	**2.30**	**0.22**	**0.31**	**0.261**	**0.093**
N2N9	**2.56**	**1.16**	**2.49**	**0.25**	**0.18**	**0.205**	**0.092**
N1N5	**2.76**	**1.24**	**2.61**	**0.29**	**0.13**	**0.149**	**0.099**
N1N4	**2.47**	**1.01**	**2.41**	**0.45**	**0.39**	**0.227**	**0.080**
N9N10	**2.30**	**0.84**	**3.32**	**0.62**	**1.64**	**0.286**	**0.080**
N1N10	**2.86**	**1.04**	**2.22**	**0.78**	**0.15**	**0.185**	**0.097**

The calculated results of the six molecules that satisfy both Eqs. (1) and (2) are summarized in **Table 4.** Their diversified structures indicate multiple possibilities to tune diradical and tetraradical characters to meet the two energy criteria. This diversity is of critical importance for future research in designing optoelectronic materials. Therefore, each of the six SF chromophore candidates shall be studied in detail. And this is the theme of this section.

We start our discussion with N1N2. **Figure 6**(d) shows that the NN π interaction is significantly weaker than the CN and CC counterparts. This is the foundation of the high diradical character (n_{LUNO} = 0.261) of N1N2, whose N centers are adjacent. The frontier natural orbitals (**Figure 12**(a)-(d)) of N1N2 undoubtedly points to the diradical character residing on the two N centers. The large diradical character leads to the low $E(T_1)$ = 0.99 eV. The tetraradical character is low since the secondary diradical character arises from the strongly π coupled C3 and C4 centers (**Figure 12**(e)). With the low $E(T_1)$, this molecule easily satisfies Eqs. (1) and (2). One question

arises. Why N2N3, which also consists of adjacent N centers, has the highest E(T_1) among all the investigated molecules? The two N centers in N2N3 are π coupled to C1 and C4 instead of each other. The couplings are exceptionally strong since C1 and C4 are only weakly coupled to the aromatic naphthalenyl fragment of the right and central rings (**Figure 9**(e)). In N1N2, the N centers are only weakly coupled to the remaining C fragments: the same aromatic napthalenyl fragment and the C3C4 vinyl fragment. The two N centers are then forced to interact with each other, despite the weak NN π interaction.

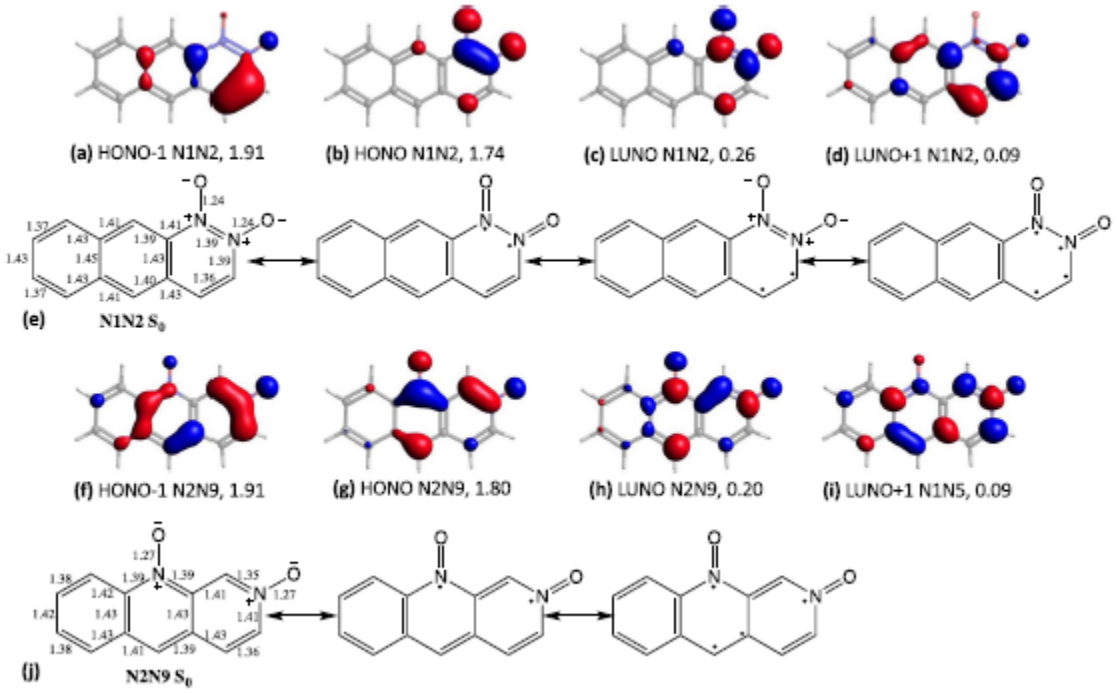

Figure 12: Frontier natural orbitals, bond lengths (in Å), and the resonance structures of N1N2 and N2N9. Occupancies of the natural orbitals are given their plottings. Adapted from *J. Chem. Phys.* 2022, *156*, 034303, copyright 2022 American Institute of Physics.

The frontier natural orbitals of N2N9 (**Figure 12**(f)-(i)) show diradical character on a butadienyl-like fragment with the two N centers at the termini. The secondary diradical fragment is the C4*a*C10 vinyl moiety. Such a tetraradical resonance structure in **Figure 12**(j) can be viewed

as arising from the diradical of the N9C8*a*C5*a*C10 butadienyl-like fragment and the diradical in the right ring, with the radical centers at the para positions of N2 and C4*a*. In this view, each of the N centers stabilizes one diradical fragment. With the two N centers synergistically stabilizing the N2C1C1*a*N9 butadienyl-like diradical character, N2N9 has a large diradical character (n_{LUNO} = 0.20) and a low E(T_1) = 1.16 eV that satisfies both criteria.

N1N5 has a relatively low diradical character at its S_0 structure (n_{LUNO} = 0.149) and a high vertical E(T_1) = 1.79 eV. The frontier natural orbitals in **Figure 13**(a)-(d) show that the diradical character of this molecule arises from the C2N1C1*a*C9 and C6N5C5*a*C10 butadienyl fragments (**Figure 13**(e)). The N centers are not even in the terminal positions of the two fragments and thus provide little stabilization of the diradical structures, explaining the low n_{LUNO} and high E(T_1). However, N1N5 features the largest $\lambda(T_1)$ = 0.56 eV among all the di-NO-substituted anthracenes. It is this large $\lambda(T_1)$ that makes it satisfy the two criteria. The HONO (highest occupied natural orbital) and LUNO (lowest unoccupied natural orbital) of the T_1 state at the T_1 optimized structure (**Figure 13**(f) and (g)) point to the diradical structure in **Figure 13**(h), which consists of two allyl-like radical fragments. Each of the allyl fragments is stabilized by one N center. Such a substantial difference between diradical characters in the S_0 to T_1 states drives the significant structural reorganization and results in the large $\lambda(T_1)$.

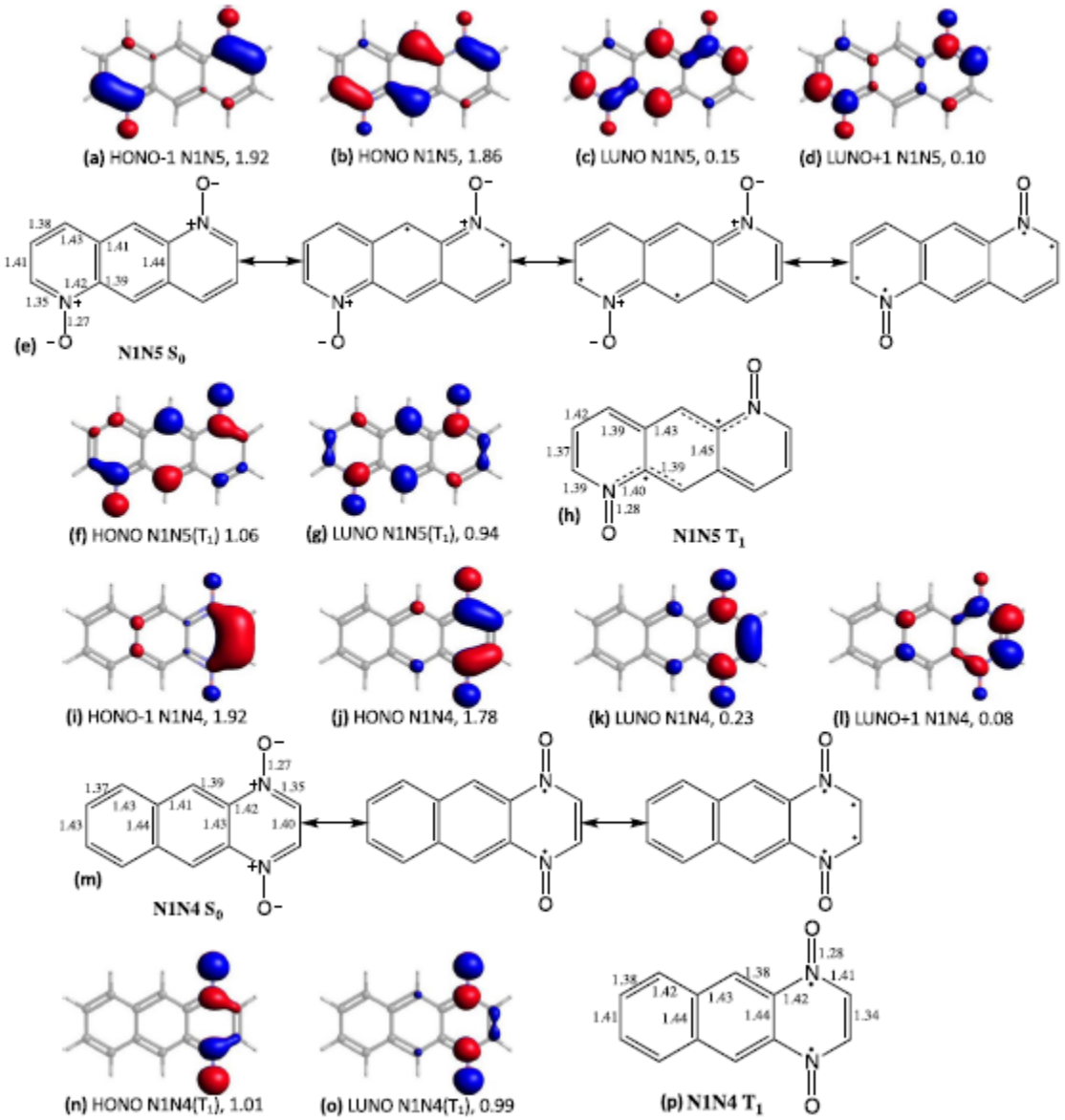

Figure 13: Frontier natural orbitals, bond lengths (in Å), and resonance structures of N1N5 and N1N4. Occupancies of the natural orbitals are given under their plottings. "(T_1)" in (f)-(h) and (n)-(p) indicate that those orbitals and bond lengths were obtained at the T_1 optimized structures of the molecules. Adapted from *J. Chem. Phys.* 2022, *156*, 034303, copyright 2022 American Institute of Physics.

N1N4 exhibits diradical character on the N1C2C3N4 butadienyl-like fragment (see natural orbitals in **Figure 13**(i)-(l), resonance structures in **Figure 13**(m)), with the two N stabilizing centers at the termini. This is similar to the diradical fragment in N2N9. The two molecules have

similar n_{LUNOS}, 0.20 and 0.23. The leftover C fragment in N1N4 is an aromatic napthalenyl moiety, which helps stabilize the diradical fragment by not coupling to it. The S_0-to-T_1 structural reorganization mainly occurs in the butadienyl-like fragment (**Figure 13**(p)). The concentration of the diradical character on the two N centers (see HONO and LUNO in **Figure 13**(n) and (o)) and the structural reorganization (**Figure 13**(p) vs (m)) mutually drive each other. The resultant 1.01 eV low $E(T_1)$ satisfies the two criteria. The similarity between N1N4 and N2N9 was not obvious to us, until we analyzed their natural orbitals and diradical characters.

N9N10 has the lowest $E(T_1)$ = 0.84 eV among all the investigated molecules. This is not surprising, as the N centers take the positions where the diradical character is most pronounced in anthracene (see **Figure 4**). The N centers hence provide the maximum stabilization for the diradical character of the pristine structure. As shown by the HONO and LUNO in **Figure 14**(b) and (c), the diradical character of N9N10 is concentrated on the two N centers. This is especially so in the T_1 state at the T_1 optimized structure, whose HONO and LUNO (**Figure 14**(f) and (g)) only reside on the N centers. The two side rings of the T_1 optimized structures have all their bond lengths close to 1.40 Å, typical for aromatic sextets. The HONO-1 and LUNO+1 in **Figure 14**(a) and (d) point to the secondary diradical character at the C1*a*N9C8*a* and C4*a*N10C5*a* allyl-like fragments (**Figure 14**(e)). Taking the central positions of the allyl-like fragments, the N centers do not provide any stabilization to the allyl-like fragments. Correspondingly, N9N10 has the highest $E(T_2)$ = 3.32eV in the present work. With the low $E(T_1)$, N9N10 easily satisfies the two criteria, with highly positive $\Delta_{SF}^{(1)}$ = 0.62 eV and $\Delta_{SF}^{(2)}$ = 1.64 eV.

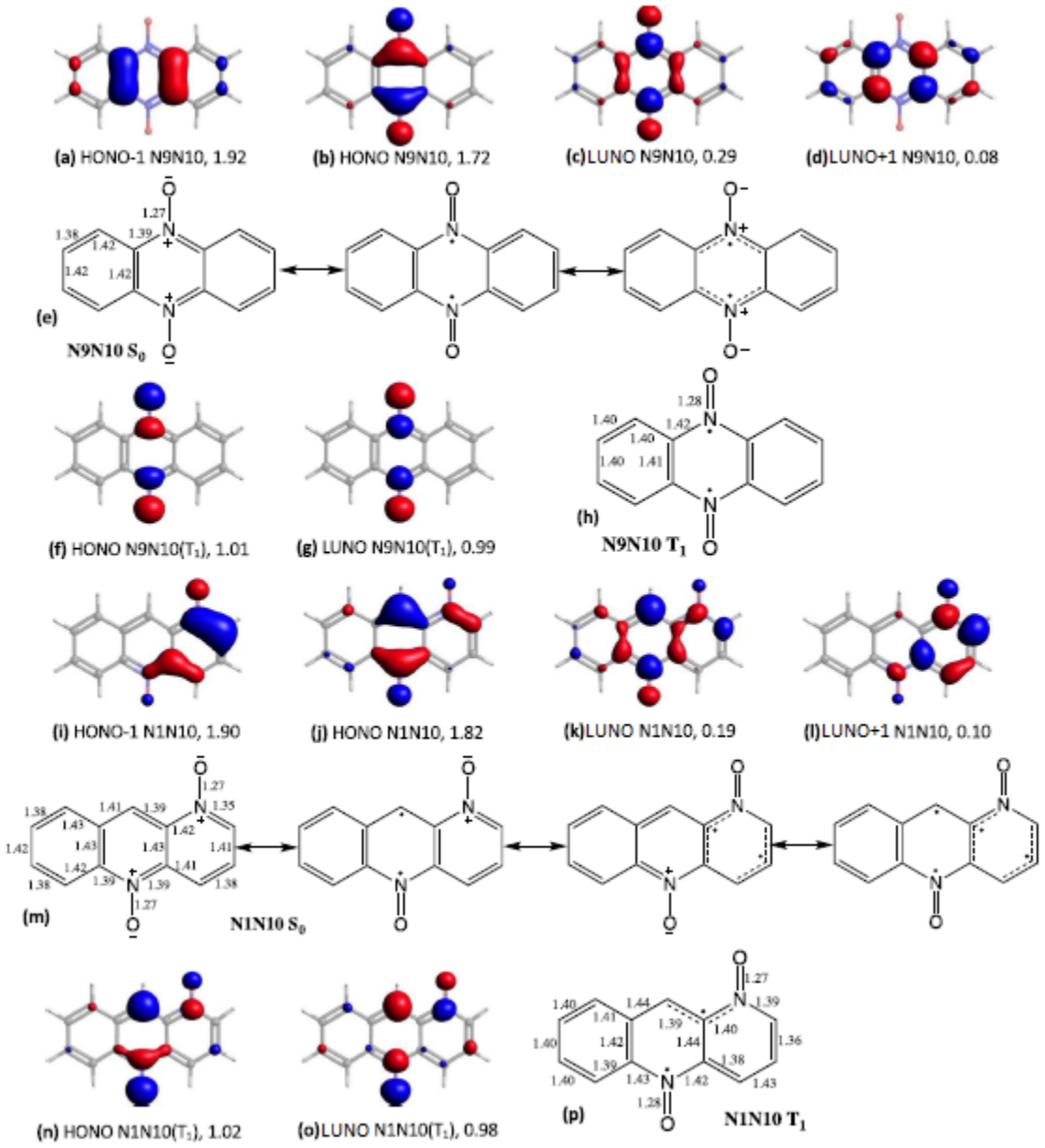

Figure 14: Frontier natural orbitals, bond lengths (in Å), and resonance structures of N9N10 and N1N10. Occupancies of the natural orbitals are given under their plottings. "(T_1)" in (f)-(h) and (n)-(p) indicate that those orbitals and bond lengths were obtained at the T_1 optimized structures of the molecules. Adapted from *J. Chem. Phys.* 2022, *156*, 034303, copyright 2022 American Institute of Physics.

The frontier natural orbitals of N1N10 (**Figure 14**(i)-(l)) indicate a diradical character concentrated at positions 9 and 10, similar to that of N9N10. The secondary diradical character is on the two allyl-like fragments at the right ring (**Figure 14**(m)). The N1C1*a*C4*a*N10 fragment seems to form a butadienyl-like diradical, with the synergic stabilization of the two N centers. However, such a butadienyl-like fragment comes with an aromatic sextet in the left ring, a radical C9, and a C2C3C4 allyl radical fragment. It is hence more convenient to have the primary diradical character shown in **Figure 14**(e), which is only stabilized by one N center at position 10. There is a significant change of the diradical character in the T_1 excitation. The HONO and LUNO in **Figure 14**(n) and (o) show diradical character at the N10 position and the N1C1*a*C9 allyl-like fragment (**Figure 14**(p)). Since N1 is a terminus of the allyl-like fragment, it stabilizes the radical fragment and contributes to stabilizing the diradical character. The two N centers hence provide synergic stabilization of the T_1 diradical character. The 0.44 eV large $\lambda(T_1)$ is consistent with the different diradical characters at the S_0 and T_1 optimized structures. While N1N10 satisfies Eq. (1) already without the structural reorganization (vertical $\Delta_{SF}^{(1)}$ = 0.17 eV), the large $\lambda(T_1)$ is the key for satisfying Eq. (2). $\Delta_{SF}^{(2)}$ changes from -0.51 to 0.15 eV after T_1 and T_2 structural reorganizations are considered. N1N10 features the lowest $E(T_2)$ among the 15 di-NO-substituted anthracenes, both vertical and 0-to-0 (2.45 and 2.22 eV). This is due to the synergic stabilization of tetraradical character by the two N centers, which also synergically stabilizes the T_1 diradical state.

3.6: A Brief Summary of the 15 Investigated Molecules

A clear difference between the six molecules that are introduced in the previous subsection and the rest is the synergic stabilization of diradical character by the two N centers. This synergic stabilization occurs only when the N centers are introduced in the appropriate positions. If the N centers stabilize two different diradical fragments, like N2N10, N1N8, and N1N6 in **Figure 11**,

they tend to induce higher tetraradical character and lower diradical character, resulting in a negative $\Delta_{SF}^{(2)}$. The aromaticity of the leftover C fragment(s), i.e., the napthalenyl fragment in N1N2 and N1N4, the left aromatic sextet in N2N9 and N1N10, and the left and right sextets in N9N10, also contribute to the synergic stabilization. Note that the synergic stabilization may only occur in the T_1 state. N1N5 and N1N10 are two such examples. For those with the synergic stabilization in S_0 already, the synergic stabilization is enhanced in T_1, as the singly occupied natural orbitals are more concentrated at the N centers. N1N4 and N9N10 are two such examples. The substantial changes of diradical character from S_0 to T_1 reflect the qualitative nature of the two sites model, which assumes frozen orbitals in all relevant excited states. The substantial changes of diradical character in S_0-to-T_1 excitation also drive substantial structural reorganizations and lead to large $\lambda(T_1)$s. The synergic stabilization and the possible large $\lambda(T_1)$s result in the lower $E(T_1)$s of the six molecules, when compared to the others, except the special case of N1N9.

The six molecules, satisfying the two energy criteria, are SF chromophore candidates. While the six molecules have low enough $E(T_1)$s to satisfy the two energy criteria, their $E(T_1)$ absolute values are not that low, ranging from 0.84 to 1.23 eV. They are close to the optimal value of 1 eV for SF chromophores. N1N2, N2N9, and N1N5 have smaller $\Delta_{SF}^{(1)}$s, < 0.3 eV, than the other three. The small $\Delta_{SF}^{(2)}$s imply low energy waste in SF. The smaller energy gap between the initial and final states of SF also facilitates the kinetics of conversion. N1N5 has the largest $E(T_1)$ = 1.24 eV, followed by 1.16 eV of N2N9. The high energy triplet excitons can be harvested by more acceptor materials. The high $E(T_1)$s imply stability and high open-circuit voltage as well[49]. The two molecules also feature large oscillator strengths (f = 0.147 and 0.144, respectively). Their vertical $E(S_1)$ = 2.91 and 2.78 eV, falling in the blue region of the solar spectrum with fairly high

irradiance[50]. With all these advantages, N1N5 and N2N9 appear to be superior to the other four. This is a relative comparison. The other four molecules are also promising candidates for SF. For instance, N9N10, despite its lowest E(T_1) among the six, has its E(S_1) and E(T_1) close to those of pentacene, the most investigated SF chromophore. All six candidates have their vertical E(S_1)s in the visible region of the solar spectrum, where the irradiance is not low. All their $f_{S1} > 0.1$, except N1N2, whose $f_{S1} = 0.064$, still a substantial value. The large $\Delta_{SF}^{(1)}$s of N1N10 and N9N10 may be beneficial, since they reserve more room for red-shift of E(S_1) in solid states of the chromophores, which may inverse the sign of $\Delta_{SF}^{(1)}$s if they are not large enough. We have no intention to pick the best out of the six. In the end, the more candidates we propose, the more likely N-oxyl SF chromophores will come true. Other than N1N2 and N9N10, the other four chromophore candidates have their E(S_1) > E(T_2). This may be a disadvantage since the $S_1 \rightarrow T_2$ intersystem crossings (ISCs) in the four molecules are thermodynamically favorable. However, the S_1 and T_2 states all involve π-to-π excitations. According to El-Sayed's rules[51-53], π-to-π ISC is highly inefficient, because of generally small spin-orbit coupling matrix elements between π orbitals on the same planar molecule. The small nuclear charges of the C, N, and O atoms in the molecules also do not facilitate ISC. Therefore, the E(S_1) > E(T_2) relation shall not be viewed as a critical problem of the four chromophore candidates.

More and more anthracene derivatives have been identified as SF chromophores in recent years[54-57]. The presently proposed chromophores have the following merits: (1) they have small size and can potentially be used to make lightweight mini OPV devices with high exciton density; (2) they are synthetically feasible, as detailed in the next section; (3) they are oxides already, and may not suffer further photooxidation, which is a source of instability for tetracene- and pentacene-based optoelectronic materials.

3.7: Feasibility of the Proposed Chromophores

Among the six proposed SF chromophores, N9N10 is the only one that, to the best of our knowledge, already exists in reality. It is called phenazine 5,10-dioxde or phenazine di-N-oxide, abbreviated as PNNO. In its time-resolved fluorescence experiment, PNNO exhibits a 400 ps fairly long S_1 lifetime[58]. The long-lived S_1 is beneficial for potential SF of this molecule, since it suggests the lack of significant decay channels for the singlet exciton. PNNO has been known for a long time for its anti-infective and tumor growth properties[59]. It has never been associated to optoelectronics. In this work, starting with the idea of implanting TEMPO-like radical centers in an aromatic system, we accidently found the potential use of this molecule in the OPV area. We hope that the present work will inspire photo-physicists and photo-chemists to design PV devices using PNNO as the chromophore.

PNNO can be synthesized through oxidation of the tertiary N centers of phenazine. One such oxidation reaction is shown in **Figure 15**(a), using H_2O_2 as the oxidant and the Ru(PVP) nanoparticles supported on γ-Al_2O_3 as the catalyst[60]. Oxidation of tertiary amines has been a long-lasting subject in synthetic chemistry. Other oxidants and catalysts can be used to achieve the oxidation, and more details can be seen in Ref. 65 and the references therein. The oxidation in **Figure 15**(a) is highly exoergic, as we calculated the reaction energy to be -70 kcal/mol. In calculating the reaction energy, phenazine and its dioxide were treated at the NEVPT2/cc-pVTZ level of theory, using the 10 electrons in 10 π orbitals active space. Only the ground states were included in the calculations. H_2O_2 and H_2O were treated at the MP2/cc-pVTZ level of theory. The reaction energy was corrected using the vibrational Gibbs free energies of the reactants and products at T = 298 K. This is a reasonable correction for the reaction that occurs in solution, where molecular translations and rotations are hindered.

Since the two N centers in phenazine are oxidized in a step-wise manner[60], we anticipate that the other five proposed SF chromophores can be synthesized through similar routes. Those proposed reactions are shown in **Figure 15**(b)-(f). They were all calculated to be highly exoergic, and the reaction energies fall in a range from -62 to -82 kcal/mol, not far from the -70 kcal/mol of the phenazine oxidation. This is consistent with the mechanism that the N centers are oxidized independently, and therefore, the N positions are not a key factor in determining the thermodynamics of oxidation. Furthermore, we found on SciFinder[61] that the 2N-containing precursor reactants in **Figure 15**(b)-(e) exist. The existence of the reactants, the highly negative reaction energies, and the well-established Ru-based catalyst suggest high feasibility of synthesizing N1N5, N1N4, N1N10, and N2N9. Benzo[g]cinnoline, the precursor for synthesizing N1N2, has not been known to exist yet. This is consistent with the rarity of pyridazine. However, the synthetic routes for pyridazine, may be applicable to synthesizing the benzo[g]cinnoline precursor. The synthesis of N1N2 is thus not completely infeasible.

Judging by their NEVPT2 ground state energies without ZPE energy corrections, N9N10 is the most stable among the six proposed chromophores. The others are higher in energy by 4.16 (N1N4), 5.16 (N2N9), 10.92 (N1N10), 16.76 (N1N5), and 20.10 kcal/mol (N1N2). The relative energies are plotted against the n_{LUNO}s of the six molecules in **Figure 16**. Excluding the N1N2 outlier, the other data exhibit a fairly good anti-correlation in a linear regression, i.e., a positive correlation between diradical character and thermodynamic stability. This correlation is reasonable, since the structures that better accommodate the radical character of the NO fragments should be more stable. The most stable N9N10 is the only one that features two aromatic sextets among the six, i.e., the least perturbation to the aromaticity of the pristine anthracene by introducing the NO fragments. N1N2 is the least stable despite its large diradical

character. The weak NN π interaction (see **Figure 6**(d)) and the 1,4 Pauli repulsion between the in-plane O lone pair orbitals contribute to raise the energy of N1N2, making it an outlier. Considering both the thermodynamic stability and the availability of precursor for synthesis, N1N2 is inferior to the other four yet to be made chromophores.

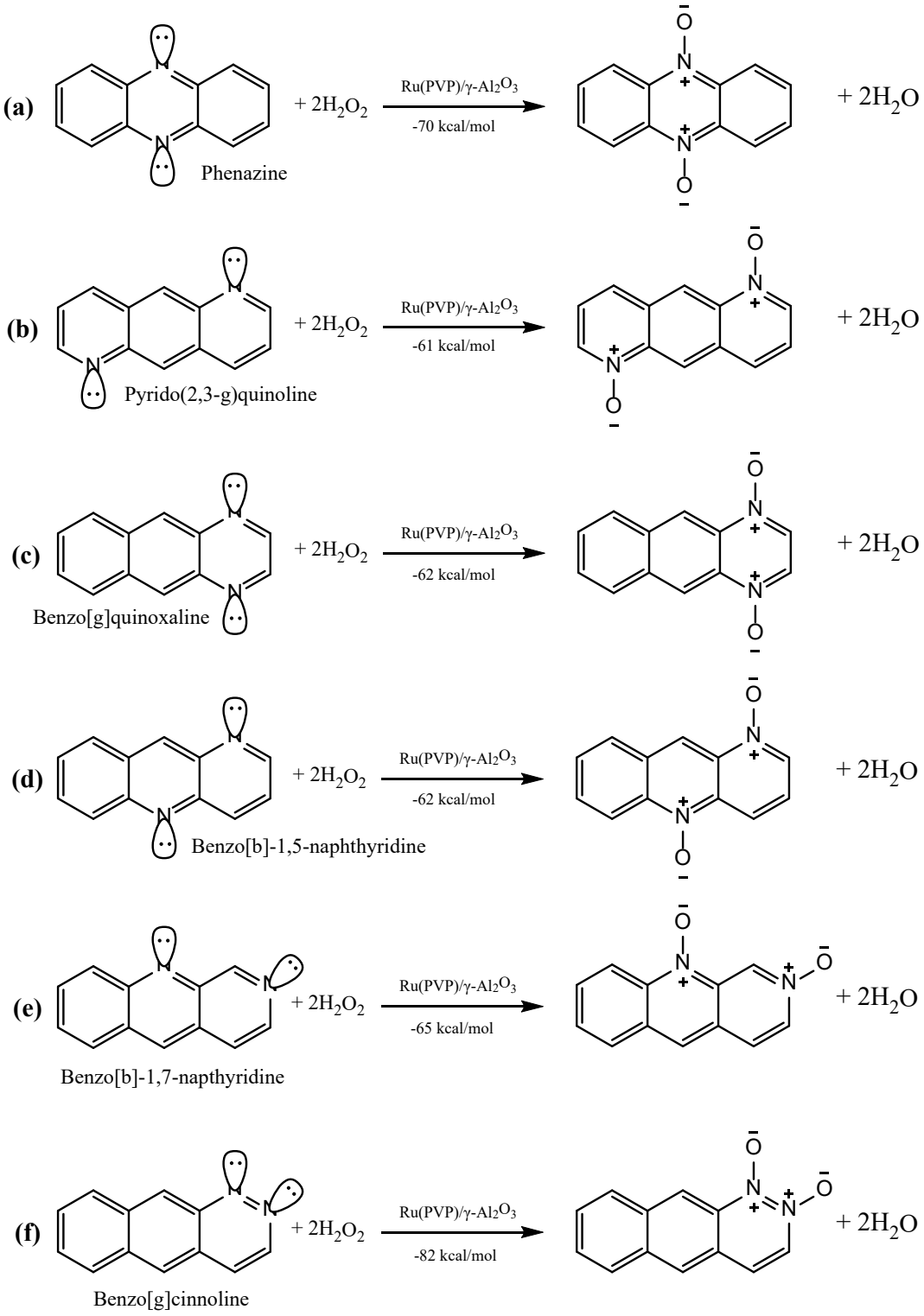

Figure 15: Reaction for N9N10 and possible reactions to synthesize the other 5 proposed SF chromophores. Given under the horizontal arrows are the calculated reaction energies

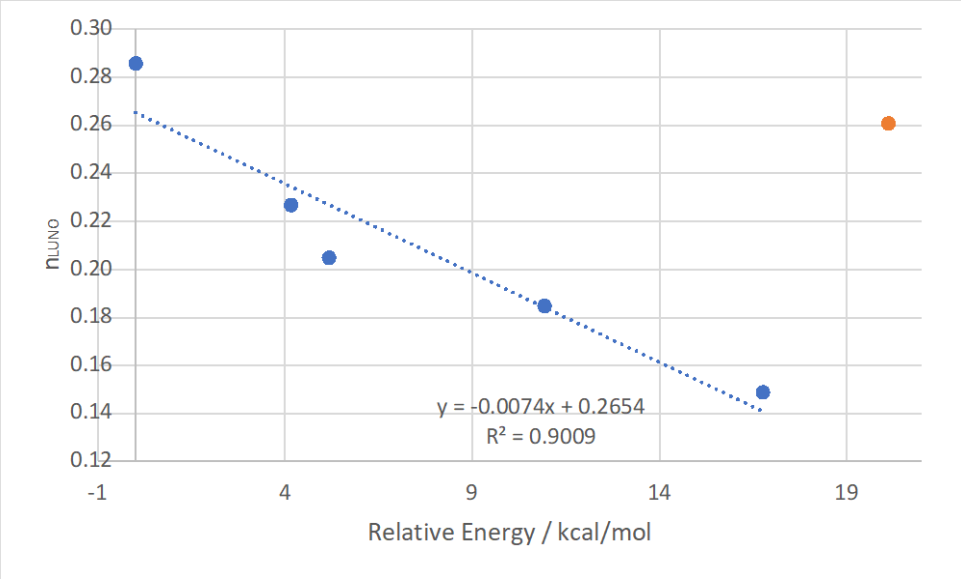

Figure 16: Correlation between relative energies and n_{LUNO}s of the six proposed good SF chromophores. The linear trend line, its equation, and the square of the correlation coefficient R^2 of the linear regression for the five blue data points are shown. Adapted from *J. Chem. Phys.* 2022, *156*, 034303, copyright 2022 American Institute of Physics.

Chapter 4: Conclusions and Future Work

In this thesis, we use computational chemistry to explore the possibility of designing singlet fission chromophores by introducing a pair of N-oxyl fragments into anthracene. The results are promising. There are in total fifteen di-N-oxyl-anthracenes. Six of them were calculated to satisfy the two key energy criteria of singlet fission: $E(S_1) > 2E(T_1)$ and $E(T_2) > 2E(T_1)$. They feature desired properties: high $E(T_1)$s, appropriate $E(S_1)$s, and good absorptions. In the six molecules, the two N-oxyl centers provide synergic stabilization of their diradical character, which is also enhanced by aromaticity of the leftover C fragments and T_1 structural organizations. The resultant substantial diradical character is responsible for those molecules satisfying the two energy criteria. Diradical character in the ground state electronic structure still provides a qualitative guidance on predicting whether the di-N-oxyl-anthracenes satisfy the energy criteria. However, the significant change of diradical character in the S_0-toT_1 excitation and possible substantial reorganization energies for S_0 to T_1 structural changes are two other important factors. We have no intention to criticize the use of diradical character as a guidance in designing singlet fission chromophores. The current strategy of introducing N-oxyl fragments into an aromatic pristine structure is inspired by this guidance. The strategy has brought a new class of singlet fission chromophores to our sight. One of the proposed SF chromophores, phenazine 5,10-dioxide (PNNO) already exists. We proposed synthetic routes for four other chromophores through similar tertiary N oxidation that is analogous to PNNO synthesis; their oxidation precursors already exist in reality. We hope that the present work will crosslink the two vibrant fields of singlet fission and aromatic NO compounds.

Based on the success of NO substitution, our attention now turns toward the large family of pre-synthesized NO di-substituted polycyclic aromatic hydrocarbons. These molecules would

have similar structure and electronics to those designed so far and are expected to be promising singlet fission chromophores. But they are even smaller. Some molecules of interest are shown below in **Figure 17**. They are di-NO-substituted naphthalenes. Pristine structures other than naphthalene are also in our radar.

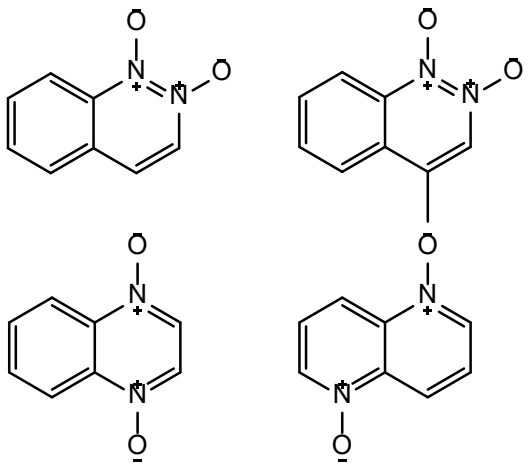

Figure 17: Chromophore candidates based on di-nitro substitution of naphthalene

References

[1] Shockley, W.; Queisser, H. J. Detailed Balance Limit of Efficiency of P-n Junction Solar Cells. *J. Appl. Phys.* 1961, *32* (3), 510–519

[2] Hanna, M. C.; Nozik, A. J. Solar Conversion Efficiency of Photovoltaic and Photoelectrolysis Cells with Carrier Multiplication Absorbers. *J. Appl. Phys.* 2006, *100* (7), 074510

[3] Singh, S.; Jones, W. J.; Siebrand, W.; Stoicheff, B. P.; Schneider, W. G. Laser Generation of Excitons and Fluorescence in Anthracene Crystals. *J. Chem. Phys.* 1965, *42* (1), 330–3425

[4] Smith, M. B.; Michl, J. Singlet Fission. *Chem. Rev.* 2010, *110* (11), 6891–6936

[5] Smith, M. B.; Michl, J. Recent Advances in Singlet Fission. *Annu. Rev. Phys. Chem.* **2013**, *64* (1), 361–386

[6] Michl, J. Unconventional Solar Energy: Singlet Fission. *Mol. Front. J.* **2019**, *03* (01), 84–91

[7] Wilson, M. W. B.; Rao, A.; Clark, J.; Kumar, R. S. S.; Brida, D.; Cerullo, G.; Friend, R. H. Ultrafast Dynamics of Exciton Fission in Polycrystalline Pentacene. *J. Am. Chem. Soc.* 2011, *133* (31), 11830–11833

[8] Scholes, G. D. Correlated Pair States Formed by Singlet Fission and Exciton-Exciton Annihilation. *J. Phys. Chem. A* **2015**, *119* (51), 12699–12705

[9] Sanders, S. N.; Pun, A. B.; Parenti, K. R.; Kumarasamy, E.; Yablon, L. M.; Sfeir, M. Y.; Campos, L. M. Understanding the Bound Triplet-Pair State in Singlet Fission. *Chem* **2019**, *5* (8), 1988–2005

[10] Miyata, K.; Conrad-Burton, F. S.; Geyer, F. L.; Zhu, X.-Y. Triplet Pair States in Singlet Fission. *Chem. Rev.* **2019**, *119* (6), 4261–4292

[11] Japahuge, A.; Zeng, T. Theoretical Studies of Singlet Fission: Searching for Materials and Exploring Mechanisms. *ChemPlusChem* **2018**, *83* (4), 146–182

[12] Casanova, D. Theoretical Modeling of Singlet Fission. *Chem. Rev.* **2018**, *118* (15), 7164–7207

[13] Ito, S.; Nagami, T.; Nakano, M. Molecular Design for Efficient Singlet Fission. *J. Photochem. Photobiol. C: Photochem. Rev.* **2018**, *34*, 85–120

[14] Zeng, T.; Hoffmann, R.; Ananth, N. The Low-Lying Electronic States of Pentacene and Their Roles in Singlet Fission. *J. Am. Chem. Soc.* **2014**, *136* (15), 5755–5764

[15] Paci, I.; Johnson, J. C.; Chen, X.; Rana, G.; Popović, D.; David, D. E.; Nozik, A. J.; Ratner, M. A.; Michl, J. Singlet Fission for Dye-Sensitized Solar Cells: Can a Suitable Sensitizer Be Found? *J. Am. Chem. Soc.* **2006**, *128* (51), 16546–16553

[16] Minami, T.; Nakano, M. Diradical Character View of Singlet Fission. *J. Phys. Chem. Lett.* **2012**, *3* (2), 145–150

[17] Minami, T.; Ito, S.; Nakano, M. Theoretical Study of Singlet Fission in Oligorylenes. *J. Phys. Chem. Lett.* **2012**, *3* (18), 2719–2723

[18] Ito, S.; Minami, T.; Nakano, M. Diradical Character Based Design for Singlet Fission of Condensed-Ring Systems with 4nπ Electrons. *J. Phys. Chem. C Nanomater. Interfaces* **2012**, *116* (37), 19729–19736

[19] Nakano, M.; Kishi, R.; Ohta, S.; Takahashi, H.; Kubo, T.; Kamada, K.; Ohta, K.; Botek, E.; Champagne, B. Relationship between Third-Order Nonlinear Optical Properties and Magnetic Interactions in Open-Shell Systems: A New Paradigm for Nonlinear Optics. *Phys. Rev. Lett.* **2007**, *99* (3), 033001

[20] Calzado, C. J.; Cabrero, J.; Malrieu, J. P.; Caballol, R. Analysis of the Magnetic Coupling in Binuclear Complexes. I. Physics of the Coupling. *J. Chem. Phys.* **2002**, *116* (7), 2728–2747

[21] Minami, T.; Ito, S.; Nakano, M. Fundamental of Diradical-Character-Based Molecular Design for Singlet Fission. *J. Phys. Chem. Lett.* 2013, *4* (13), 2133–2137

[22] Wen, J.; Havlas, Z.; Michl, J. Captodatively Stabilized Biradicaloids as Chromophores for Singlet Fission. *J. Am. Chem. Soc.* **2015**, *137* (1), 165–172

[23] Akdag, A.; Havlas, Z.; Michl, J. Search for a Small Chromophore with Efficient Singlet Fission: Biradicaloid Heterocycles. *J. Am. Chem. Soc.* **2012**, *134* (35), 14624–14631

[24] Zeng, T.; Ananth, N.; Hoffmann, R. Seeking Small Molecules for Singlet Fission: A Heteroatom Substitution Strategy. *J. Am. Chem. Soc.* **2014**, *136* (36), 12638–12647

[25] Zeng, T.; Goel, P. Design of Small Intramolecular Singlet Fission Chromophores: An Azaborine Candidate and General Small Size Effects. *J. Phys. Chem. Lett.* **2016**, *7* (7), 1351–1358

[26] Zeng, T. Through-Linker Intramolecular Singlet Fission: General Mechanism and Designing Small Chromophores. *J. Phys. Chem. Lett.* **2016**, *7* (21), 4405–4412

[27] Zeng, T.; Mellerup, S. K.; Yang, D.; Wang, X.; Wang, S.; Stamplecoskie, K. Identifying (BN)2-Pyrenes as a New Class of Singlet Fission Chromophores: Significance of Azaborine Substitution. *J. Phys. Chem. Lett.* **2018**, *9* (11), 2919–2927

[28] Japahuge, A.; Lee, S.; Choi, C. H.; Zeng, T. Design of Singlet Fission Chromophores with Cyclic (Alkyl)(Amino) Carbene Building Blocks. *J. Chem. Phys.* **2019**, *150* (23), 234306

[29] Pradhan, E.; Bentley, J. N.; Caputo, C. B.; Zeng, T. Designs of Singlet Fission Chromophores with a Diazadiborinine Framework. *ChemPhotoChem* **2020**, *4* (11), 5279–5287

[30] El Bakouri, O.; Smith, J. R.; Ottosson, H. Strategies for Design of Potential Singlet Fission Chromophores Utilizing a Combination of Ground-State and Excited-State Aromaticity Rules. *J. Am. Chem. Soc.* **2020**, *142* (12), 5602–5617

[31] Fallon, K. J.; Budden, P.; Salvadori, E.; Ganose, A. M.; Savory, C. N.; Eyre, L.; Dowland, S.; Ai, Q.; Goodlett, S.; Risko, C.; Scanlon, D. O.; Kay, C. W. M.; Rao, A.; Friend, R. H.; Musser, A. J.; Bronstein, H. Exploiting Excited-State Aromaticity to Design Highly Stable Singlet Fission Materials. *J. Am. Chem. Soc.* **2019**, *141* (35), 13867–13876

[32] Baranac-Stojanović, M. Triplet-State Structures, Energies, and Antiaromaticity of BN Analogues of Benzene and Their Benzo-Fused Derivatives. *J. Org. Chem.* **2019**, *84* (21), 13582–13594

[33] Ito, S.; Nakano, M. Theoretical Molecular Design of Heteroacenes for Singlet Fission: Tuning the Diradical Character by Modifying π-Conjugation Length and Aromaticity. *J. Phys. Chem. C Nanomater. Interfaces* **2015**, *119* (1), 148–157

[34] Pradhan, E.; Lee, S.; Choi, C. H.; Zeng, T. Diboron- and Diaza-Doped Anthracenes and Phenanthrenes: Their Electronic Structures for Being Singlet Fission Chromophores. *J. Phys. Chem. A* **2020**, *124* (40), 8159–8172

[35] Clar, E. The Aromatic Sextet; Wiley: New York, 1972

[36] Anthony, J. E. Functionalized Acenes and Heteroacenes for Organic Electronics. *Chem. Rev.* **2006**, *106* (12), 5028–5048

[37] Anthony, J. E. The Larger Acenes: Versatile Organic Semiconductors. *Angew. Chem. Int. Ed Engl.* **2008**, *47* (3), 452–483

[38] Nutting, J. E.; Rafiee, M.; Stahl, S. S. Tetramethylpiperidine N-Oxyl (TEMPO), Phthalimide N-Oxyl (PINO), and Related N-Oxyl Species: Electrochemical Properties and Their Use in Electrocatalytic Reactions. *Chem. Rev.* **2018**, *118* (9), 4834–4885

[39] Becke, A. D. Density-functional Thermochemistry. I. The Effect of the Exchange-only Gradient Correction. *J. Chem. Phys.* **1992**, *96* (3), 2155–2160

[40] Lee, C.; Yang, W.; Parr, R. G. Development of the Colle-Salvetti Correlation-Energy Formula into a Functional of the Electron Density. *Phys. Rev. B Condens. Matter* **1988**, *37* (2), 785–789

[41] Dunning, T. H., Jr. Gaussian Basis Sets for Use in Correlated Molecular Calculations. I. The Atoms Boron through Neon and Hydrogen. *J. Chem. Phys.* **1989**, *90* (2), 1007–1023

[42] Angeli, C.; Cimiraglia, R.; Evangelisti, S.; Leininger, T.; Malrieu, J.-P. Introduction Ofn-Electron Valence States for Multireference Perturbation Theory. *J. Chem. Phys.* **2001**, *114* (23), 10252–10264

[43] Angeli, C.; Cimiraglia, R.; Malrieu, J.-P. N-Electron Valence State Perturbation Theory: A Fast Implementation of the Strongly Contracted Variant. *Chem. Phys. Lett.* **2001**, *350* (3–4), 297–305

[44] Angeli, C.; Cimiraglia, R.; Malrieu, J.-P. N-Electron Valence State Perturbation Theory: A Spinless Formulation and an Efficient Implementation of the Strongly Contracted and of the Partially Contracted Variants. *J. Chem. Phys.* **2002**, *117* (20), 9138–9153

[45] Koldasheva, E. M.; Strelets, V. V.; Geletii, Y. V.; Shestakov, A. F.; Tse, Y.-K. Phenazinee Di-N-Oxide Radical Cation and Its Reactions with Hydrocarbons. *Russ. Chem. Bull.* **1996**, *45* (8), 1889–1895

[46] Schmidt, M. W.; Baldridge, K. K.; Boatz, J. A.; Elbert, S. T.; Gordon, M. S.; Jensen, J. H.; Koseki, S.; Matsunaga, N.; Nguyen, K. A.; Su, S.; Windus, T. L.; Dupuis, M.; Montgomery, J. A. General Atomic and Molecular Electronic Structure System. *J. Comput. Chem.* **1993**, *14* (11), 1347–1363

[47] M. S. Gordon and M. W. Schmidt, in Advances in Electronic Structure Theory: GAMESS a Decade Later (Elsevier, Amsterdam, 2005), Chap. 41, pp. 1167–1189.

[48] Neese, F. The ORCA Program System: The ORCA Program System. *Wiley Interdiscip. Rev. Comput. Mol. Sci.* **2012**, *2* (1), 73–78

[49] Lee, J.; Jadhav, P.; Reusswig, P. D.; Yost, S. R.; Thompson, N. J.; Congreve, D. N.; Hontz, E.; Van Voorhis, T.; Baldo, M. A. Singlet Exciton Fission Photovoltaics. *Acc. Chem. Res.* **2013**, *46* (6), 1300–1311

[50] P. Wurfel, Physics of Solar Cells: From Basic Principles to Advanced Concepts (Wiley-VCH Verlag, Weinheim, 2009).

[51] Lower, S. K.; El-Sayed, M. A. The Triplet State and Molecular Electronic Processes in Organic Molecules. *Chem. Rev.* **1966**, *66* (2), 199–241

[52] El-Sayed, M. A. Triplet State. Its Radiative and Nonradiative Properties. *Acc. Chem. Res.* **1968**, *1* (1), 8–16

[53] Pokhilko, P.; Krylov, A. I. Quantitative El-Sayed Rules for Many-Body Wave Functions from Spinless Transition Density Matrices. *J. Phys. Chem. Lett.* **2019**, *10* (17), 4857–4862

[54] Bhattacharyya, K.; Datta, A. Polymorphism Controlled Singlet Fission in TIPS-Anthracene: Role of Stacking Orientation. *J. Phys. Chem. C Nanomater. Interfaces* **2017**, *121* (3), 1412–1420

[55] Bae, Y. J.; Christensen, J. A.; Kang, G.; Zhou, J.; Young, R. M.; Wu, Y.-L.; Van Duyne, R. P.; Schatz, G. C.; Wasielewski, M. R. Substituent Effects on Energetics and Crystal Morphology Modulate Singlet Fission in 9,10-Bis(Phenylethynyl)Anthracenes. *J. Chem. Phys.* **2019**, *151* (4), 044501

[56] Nagami, T.; Okada, K.; Miyamoto, H.; Yoshida, W.; Tonami, T.; Nakano, M. Molecular Design Principle for Efficient Singlet Fission Based on Diradical Characters and Exchange Integrals: Multiple Heteroatom Substitution Effect on Anthracenes. *J. Phys. Chem. C Nanomater. Interfaces* **2020**, *124* (22), 11800–11809

[57] Stoycheva, J.; Tadjer, A.; Garavelli, M.; Spassova, M.; Nenov, A.; Romanova, J. Boron-Doped Polycyclic Aromatic Hydrocarbons: A Molecular Set Revealing the Interplay between Topology and Singlet Fission Propensity. *J. Phys. Chem. Lett.* **2020**, *11* (4), 1390–1396

[58] Shi, X.; Poole, J. S.; Emenike, I.; Burdzinski, G.; Platz, M. S. Time-Resolved Spectroscopy of the Excited Singlet States of Tirapazamine and Desoxytirapazamine. *J. Phys. Chem. A* **2005**, *109* (8), 1491–1496

[59] Viktorsson, E. Ö.; Aesoy, R.; Støa, S.; Lekve, V.; Døskeland, S. O.; Herfindal, L.; Rongved, P. New Prodrugs and Analogs of the Phenazine 5,10-Dioxide Natural Products Iodinin and Myxin Promote Selective Cytotoxicity towards Human Acute Myeloid Leukemia Cells. *RSC Med Chem* **2021**, *12* (5), 767–778

[60] Veerakumar, P.; Balakumar, S.; Velayudham, M.; Lu, K.-L.; Rajagopal, S. Ru/Al2O3 Catalyzed N-Oxidation of Tertiary Amines by Using H2O2. *Catal. Sci. Technol.* **2012**, *2* (6), 1140

[61] We did structure searches for the 2N-containing precursor reactants in **Figure 15**(b)-(f) on http://scifinder.cas.org/. Those in **Figure 15**(b)-(e) were found to be synthesized already.